OXIDATION AND RELEASE OF RUTHENIUM IN HIGH TEMPERATURE AIR

Lajos Matus, Oleg Prokopiev, Bálint Alföldy,
Anna Pintér, Zoltán Hózer
KFKI Atomic Energy Research Institute
H-1525 Budapest 114, P.O.B. 49, Hungary
e-mail: hozer@sunserv.kfki.hu

Budapest, November 2002

Projekt: Project:	PHEBUS FP PROGRAMME
Cím: Title:	**OXIDATION AND RELEASE OF RUTHENIUM IN HIGH TEMPERATURE AIR**
Készítette: Authors:	Lajos Matus, Oleg Prokopiev, Bálint Alföldy, Anna Pintér, Zoltán Hózer
Dokumentum típus: Type of the document:	Deliverable No. 1.

Módosítás/ Revision	**Kelt/** Date	**Aláírások/** Signatures		
		Készítette/ Authors	**Átvizsgálta/** Reviewed by	**Jóváhagyta/** Approved by
0.	01.12.2002	L. Matus	Z. Hózer	I. Vidovszky
1.				
2.				
3.				

Módosítás / Revision **Kelt /** Date	**A módosítás rövid leírása** Short description of the revision
1.	
2.	
3.	

Contents

1. INTRODUCTION

In the late phase of a severe accident - if the bottom of high pressure vessel is failed - air can get into the core area. The air streaming in will strongly oxidize the high temperature fuel elements. Under air oxidation large amount of volatile ruthenium oxides are escaping, as can be concluded from some experiments modeling the air ingress [1,2,3,4,5].

The fission product ruthenium is in the spent up fuel as metal forming alloys with Rh, Pd, Mo and Tc. Both the radioactive [103]Ru and [106]Ru decay with β^- emission to [103]Rh and [106]Rh with half life of 39.26 and 374 days, respectively.

Ru is one of the fission product elements with highest concentration and it rises troubles at the deposition of spent up fuels as well (100 g UO_2 at 44 GWd/tU burn up level contains 0.5 g FP ruthenium [6.].) About 60 % of β^- activity of waste deposits is coming from ruthenium isotopes [7,8]. The Chernobyl accident 16 years ago called the attention to another severe environmental problem. The investigations after the accident proved, that the atmospheric and soil surface concentration of ruthenium isotopes are as high as that of ^{131}I and [137]Cs [9-11]. Similar results were coming from the investigations of other, not so severe accidents [12].

The diffusion of Ru in UO_2 is low, under 2000°C the ruthenium escapes only from the gap and surface of pellets, moreover from layer near to the surface in an atmosphere containing free oxygen [13]. The balance regarding the release of Ru from the core of Chernobyl NPP showed about 3 % release of the total FP ruthenium inventory [14]. The ruthenium release and its mobility in the environment are enhanced by the properties of the oxides. The ruthenium tetroxide is rather volatile even at room temperature. The RuO_3 volatile is as well, but exists only at high temperature (> 900 °C). In case of a severe accident with air ingress they can get out to the environment, where as gas or condensed phase on the surface of aerosol particles can be transported to large distances. The morphological investigation of aerosol particles after the Chernobyl accident showed, that they have a harmful effect by precipitation on the surface of the skin, the inhalation is not substantial [15,16].

The radioactive Ru rises serious health dangers [13]. The health effect of radioactive ruthenium on short term is similar to the iodine, on longer term is like the cesium [14]. The [106]Ru with its longer half life rise the probability of cancer. It does not accumulate into any organ, dislike to the iodine in the thyroid gland or strontium in the bones, but it has a harmful effect for the whole body, mainly in the lungs and digestion organs.

In the frame of investigations dealing with the severe accidents the ruthenium got a substantial attention. In one of the experimental series small size burned out fuel pellet pieces were studied in separate effect tests regarding the rate of air oxidation of uranium-dioxide and the escape of ruthenium [13]. However these tests resulted only poor information about the detailed effect of gas environment, the longer escape routes and the influence of lower temperature stages.

After the Chernobyl accident the KFKI Radiation Protection Department, like many other research sites, gathered aerosol particles with higher radioactivity. They found that all of the particles contained ruthenium, in some of them the activity was coming entirely from ruthenium isotopes [23].

The CODEX-AIT (COre Degradation Experiments - Air Ingress Test) experiments performed earlier in our laboratory indicated substantially faster degradation of core components in air compared to steam. The fuel elements contained only fresh fuel rods, accordingly no information regarding the fission product release was achieved. In the PHEBUS FP program a severe accident modeling test (FPT-5) is planned with irradiated fuel rods and air ingress circumstances. In this case the fission product release can be judged as well. The preparatory work of this experiment may be supported by the small size test results of the present work.

The aim of the present test program was to get data for assessment of ruthenium release at severe accident with air ingress. The factors influencing the oxidation and release processes were studied. The investigation of movement of ruthenium with high temperature air was one of the main goals of the tests. At the first series of the experiments only Ru powder was used in ZrO_2 matrix. Later other fission product elements were mixed into the test material. At the last series UO_2 component were added together with the fission products. The investigations approach to the real fuel conditions stepwise to get information about the influence of different components. However retention effect of UO_2 was not included into the studies.

The present work was performed with the financial support of the Hungarian Atomic Energy Commission. The program was discussed with the experts of the IRSN and JRC in order to produce information useful for the PHEBUS FP project. The discussions and visit of PHEBUS experts clarified some demands regarding the performance of tests and evaluation of data to be achieved. The consultations enlarged the scope of the information to get out and some of them were included already in this year program. The study of the retention effect of UO_2 is in the next year program.

The list of investigated systems with the parameters is summarized in the next (in parentheses are the identification numbers of experiments):

a./ Ru powder in ZrO_2 matrix, influence of:
- influence of air streaming rate (Ru1, Ru4 and Ru5),
- the temperature of reaction chamber (Ru5, Ru6, Ru8),
- cladding material (Ru10),
- stainless steal in the decreasing temperature stage (Ru7),
- steam content of air (Ru9, Ru12, Ru15, Ru17),
- Ru escape in time (Ru13, Ru14, Ru15, Ru16),
- filtering of aerosols (Ru13).

b./ Ru powder in ZrO_2 matrix with other fission products,
- dry air, differential collection of precipitates (Ru16),
- wet air, differential collection of precipitates (Ru15),
- wet air, integral collection of precipitates (Ru17).

c./ Ru powder in ZrO_2 matrix with other fission products and UO_2 ,
- dry air (Ru18),
- wet air (Ru19).

d./ Ru powder in ZrO_2 matrix, control test for the role of oxygen,
- with dry argon (Ru11-1),
- with wet argon (Ru11-2).

Spectrophometric method with suitable sensitivity has been developed for the determination of ruthenium. Precipitations with ruthenium content have been formed in the outlet tubes and on the filters. Their Ru content were determined by XRF and SEM-EDX methods.

In Chapter 2 some physical and chemical properties of Ru and its oxides are summarized, those which are important regarding the present investigations. In Chapter 3 the experimental device and the analytical methods are shown. The results and discussions are described in Chapter 4.

2. SOME PHYSICAL AND CHEMICAL PROPERTIES OF RUTHENIUM

The ruthenium belongs to the platinum metals group, its density is 12.30 g/cm^3, melting point is 2334 °C, boiling point is 4150 °C. Ru is a gray, extremely hard, brittle material, it can be pulverized. It solves substantial amount of oxygen and hydrogen.

Chemically it is very resistant, even more than the other platinum group metals. In air on the surface of the metal in some seconds is formed a very dense RuO_2 layer and it prevents fromt the further oxidation. The thickness of RuO_2 layer is growing slowly with the temperature up to about 700 °C. At higher temperature is starting the formation of volatile RuO_3 and RuO_4, leading to the weight loss of Ru metal. At temperatures < 1000 °C RuO_4, at temperatures >1000 °C RuO_3 is the larger component. The rate of evaporation is constant, and the intensity is 1 $mg.cm^{-2}.h^{-1}$ at about 1100 °C [13].
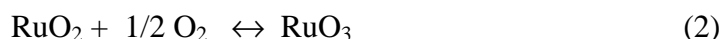
The acids solve it only if a strong oxidizing component is in the mixture, even the $HCl-HNO_3$ hardly solve it, from this point of view even more resistant as the platinum. The water solution of alkali hydroxides with chlorine content solve it by formation of ruthenates. Its most important properties from the point of view of present task:
  – its tetroxide is stable and volatile,
  – it has many oxidation stages,
  – the complex formation is very strong,
  – amphoter with easy transformation between the anionic and cationic form.

The most important ruthenium oxides are the RuO_2, RuO_3 and RuO_4. The RuO_2 is a deep blue compound. It is very stable, the oxygen pressure over it is rising to 1 bar at 1500 °C only (decomposition temperature). The RuO_3 and RuO_4 can be formed from Ru according to the next chemical processes:
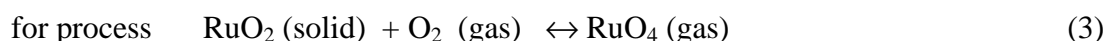
$$Ru + O_2 \leftrightarrow RuO_2 \qquad\qquad (1)$$

then

$$RuO_2 + 1/2\, O_2 \leftrightarrow RuO_3 \qquad\qquad (2)$$

and

$$RuO_2 + O_2 \leftrightarrow RuO_4 \qquad\qquad (3)$$

At lower temperatures the RuO_3 is not stable, and the chemical equilibrium will be shifted to the direction of RuO_2 and RuO_4 formation. (RuO_4 can be prepared at low temperature (50-100 °C) as well with strong oxidants ($HClO_4$, $NaBiO_3$).

The equilibrium partial pressures of RuO_3 and RuO_4 over RuO_2 have been calculated by equations published in [17] and originated from [18]. They are as follows:

for process RuO_2 (solid) $+ O_2$ (gas) $\leftrightarrow RuO_4$ (gas)   (3)

$\lg K_p = -6219.4/T + 4.2120 - 1.0315 . \lg T -0.0557E\text{-}5 * T^{-2}$ (i)

for process RuO_2 (solid) $+ 1/2\ O_2$ (gas) $\leftrightarrow RuO_3$ (gas)   (2)
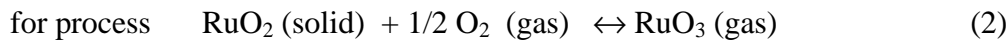
   $\lg K_p = -12968.5/T + 10.1385 - 1.2429 * \lg T - 0.1399E\text{-}3 * T + 0.033E5 * T^{-2}$ (ii)

where K_p in bars, T in Kelvin is given. Using the 21% O_2 content of air the partial pressures of the Ru-oxides is plotted in Figure1.
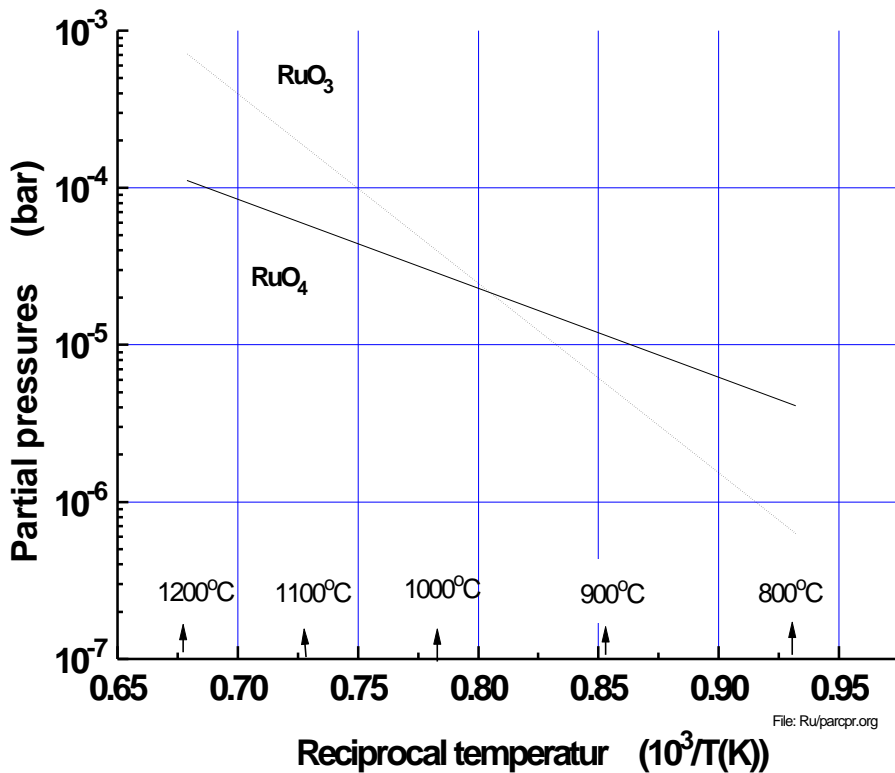

Figure 1. Partial pressures of RuO_3 and RuO_4 over RuO_2 in 1 bar air

       The joint partial pressures of RuO_3 and RuO_4 over RuO_2 were important data at the evaluation of the experimental results. From (i) and (ii) an equation was made as follows:

       $\lg P(RuO_x) = -9.81789 + 0.00562 * t(°C)$ (iii)

$P(RuO_x)$ in bars. The plotted function of joint partial pressures can be seen in Fig.2.

       At the planning of time schedule of experiments an important parameter was the evaporation rate of Ru in air. The data published in [18] were plotted in Figure 3 and the next equation was derived by fitting:

       $\lg \Delta w = 9.43818 - 12310.4/T(K)$ (iv)

where Δw is resulted in mg.cm^{-2}.h^{-1}.

10^{-3}
Joint partial pressures of RuO_3 and RuO_4
$log_{10}P_{RuO_x} = -9.81789 + 0.00562*t_{(^oC)}$

$P_{tot}(RuO_x)$

10^{-4}

10^{-5}

10^{-6}

800   **900**   **1000**   **1100**   **1200**

Temperature (^oC)

File: Rut.../parcpra3.org
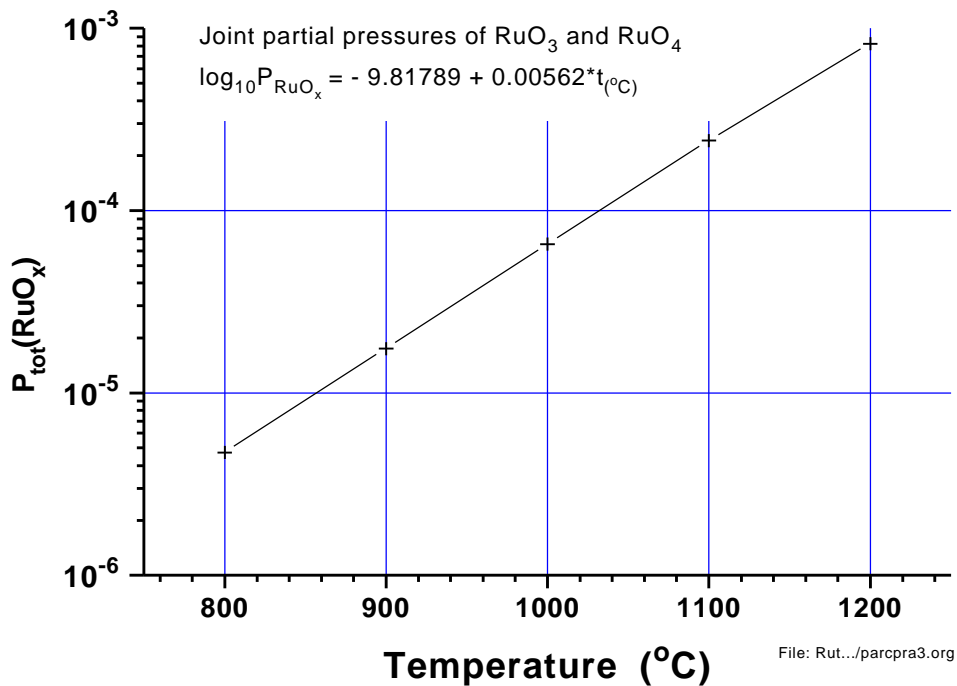
Figure 2. Joint partial pressure of RuO_3 and RuO_4 over RuO_2 at 1 bar air.

100

10

Δw $(mg*cm^{-2}*h^{-1})$

1

0.1

$log_{10} \Delta w = 9.43818 - 12310.4/T$

$1100 ^oC$

0.01

6.0 6.5 7.0 7.5 8.0 8.5

Reciprocal temperature $(10^4/T(K))$

File: rut.../totevap.org
Plot 2

Figure 3. Evaporation rate of Ru in air (weight loss)

3. EXPERIMENTAL

3.1 Oxidation setup and sampling

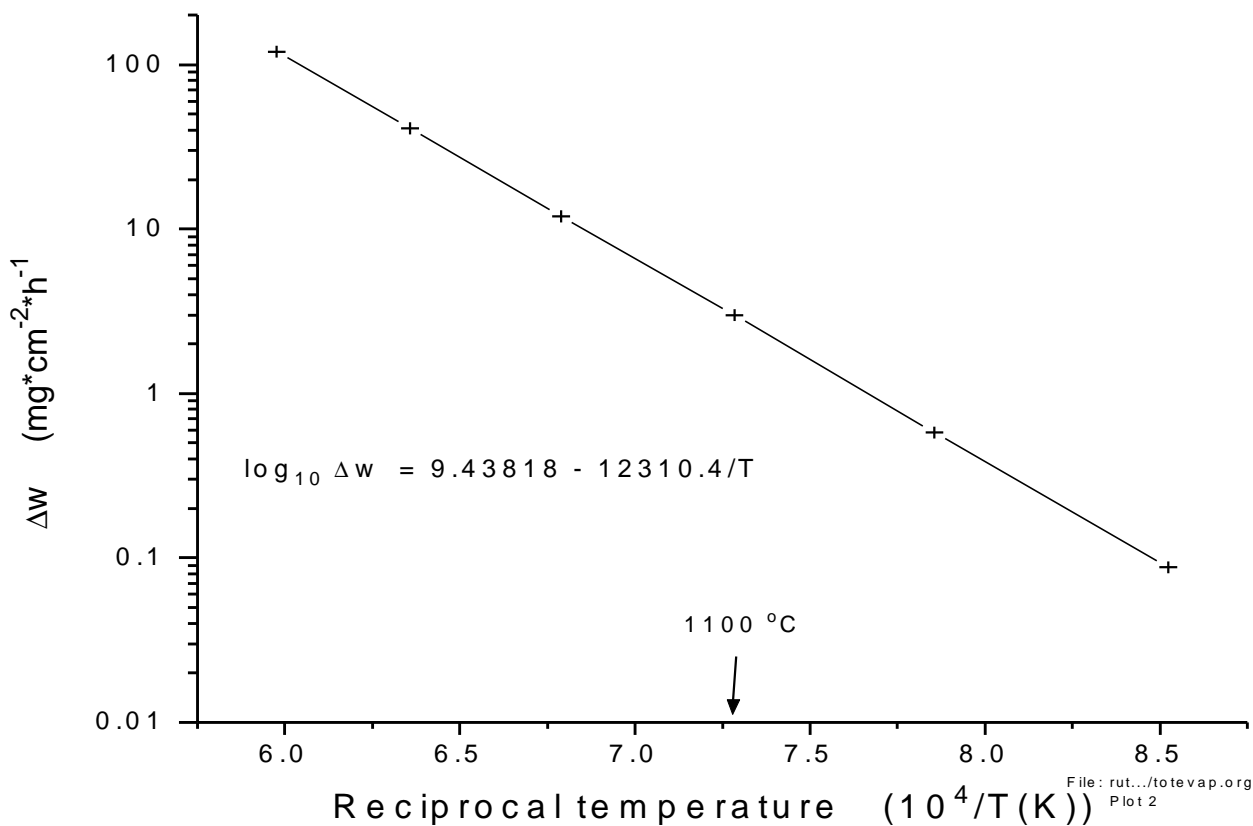The experiments were made using ZrO_2 matrix with Ru powder and later with other fission product elements and UO_2 as well. The Ru concentration applied was at the range of a middle extent burned out fuel. (44 GWd/tU, 0.005 g Ru/gUO_2). 1 g ZrO_2 with ~ 5 mg Ru powder was filled as charge into the reaction chamber. At most of the experiments the air flowrate was 3 ml/s, the evaporation of Ru was fast enough to get equilibrium partial pressures for ruthenium oxides at this streaming rate. The experiments were performed mainly at 1100 ^{o}C, when the 3 ml/s air volume rate could take away 0.15 mg/min ruthenium. The evaporation rate of 5 mg Ru powder with 5 µm particle size was estimated as 0.25 mg/min.

The scheme of experimental device is shown in Figure 4. The reaction chamber is a quartz tube with a larger diameter part at the middle. That is the reaction chamber containing the test mixture. The top of the tube connected with a flexible Teflon tube to the sampling device. The flexible gas tubing made possible to heat up the furnace in advance and only then sink the reaction chamber with the charge into the hot area.

The furnace had three independently heated stage and a joint microprocessor control for resulting 150 mm long range in the middle with about 1-2 ^{o}C stable temperature in the length and time.
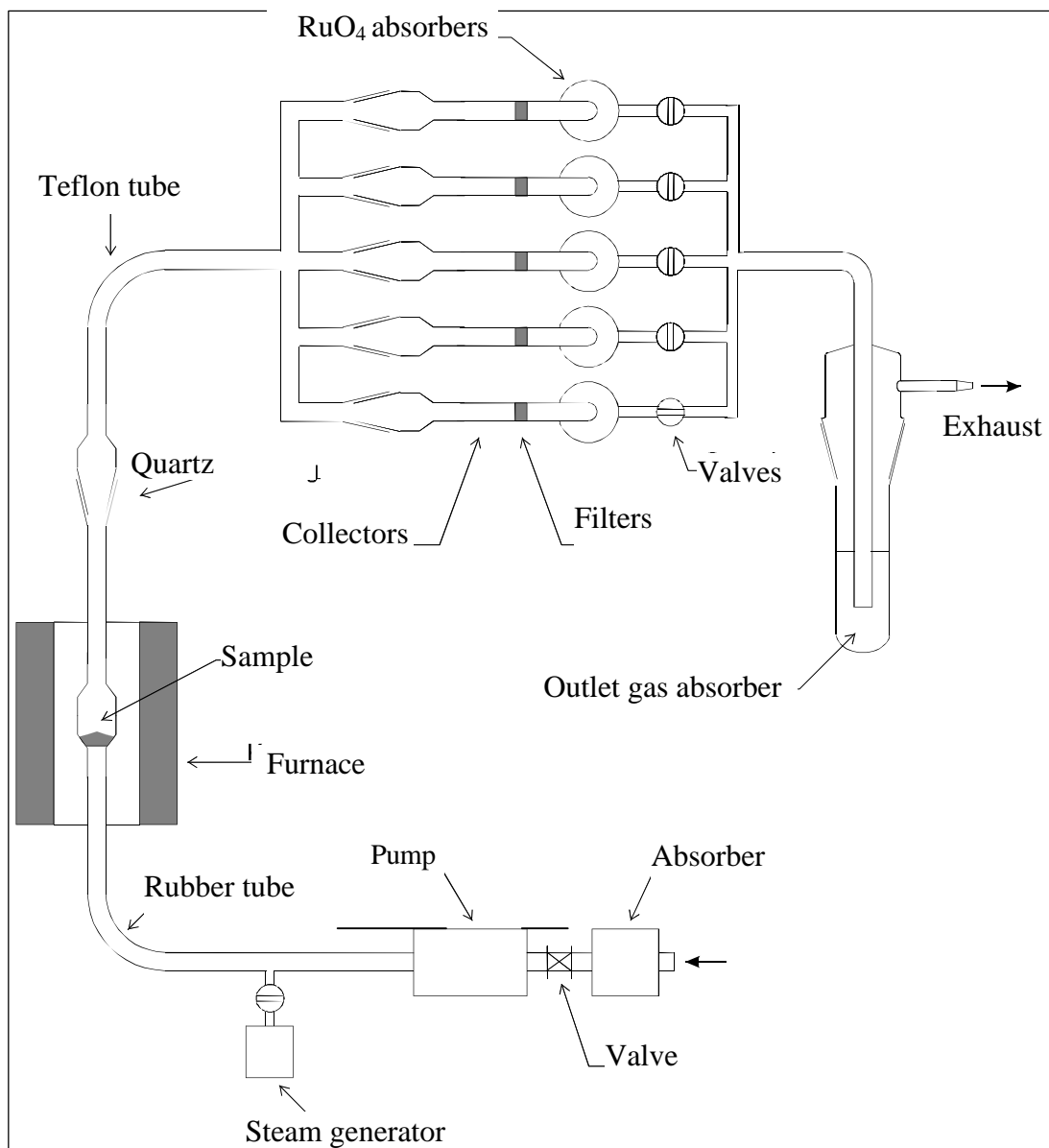
Figure 4. Scheme of experimental setup

When the temperature is sinking to the ambient level the (2) and (3) equilibrium chemical reaction of RuO_3 and RuO_4 with RuO_2 are moving toward the formation of RuO_2 and it appears as deep blue precipitation in the quartz tube at the top level of furnace decreasing temperature area. Because of the troubles with the RuO_2 solubility, an inner quartz tube was placed into the reaction chamber outlet tube at the area of precipitation. The amount of precipitation was measured by weighting of the inlet quartz tube before and after an experiment, to get information about the amount of precipitated materials. At some tests the inlet tube was changed 4-5 times during the test. With this method the precipitation process could be determined in time, resulting in information on the escape of ruthenium. The upper end of heated area was closed with a 65 mm long ceramic rod with a hole in the middle for the outlet tube of reaction chamber. The aim of this arrangement was to get a reproducible decreasing temperature stage for the determination of the precipitation extent in function of temperature and time. The decreasing temperature scale was determined with thermocouple and the results are plotted in Figure 5.
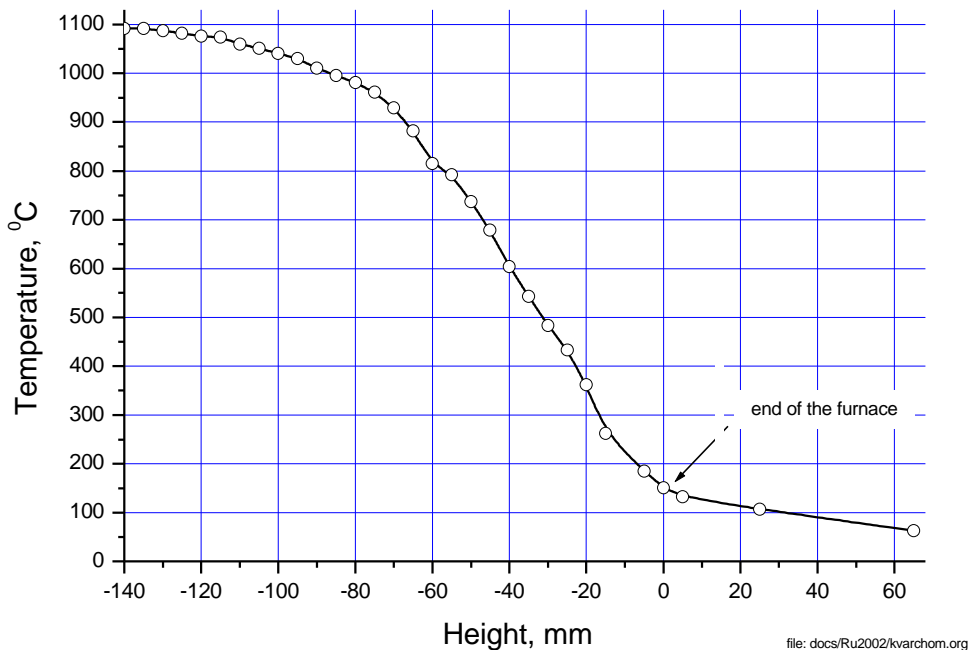
Figure 5. Thermal gradient in the upper end of furnace (ceramic rod)

The scheme of a sampling unit is shown in Figure 6. The whole sampling facility contains 5 parallel units, which were used after each other, to get data with the time. At the inlet Ni and Si plates were placed in the glass tube for collecting aerosol precipitations for SEM investigations. Moreover a quartz fibre filter was in the gas stream to separate the aerosol components. The gas ruthenium oxide components were absorbed by 1nHCl in the absorber tube. The RuO_4 was absorbed in the form of $RuCl_3.nH_2O$. To improve the efficiency of absorption the inlet tube endings in the absorber solution contained sintered glass plates.
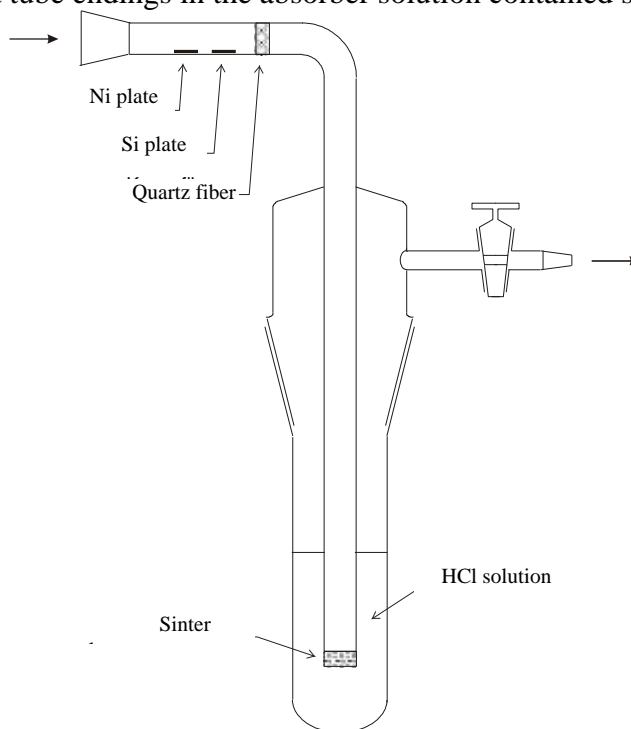
Figure 6. Scheme of sampling device

The time periods of the use of absorbers were settled so, that the release of Ru from the charge in the high temperature furnace happened during the operation of the first two samplers. The further samplers showed the Ru movement with the gas stream through the reevaporation of precipitated RuO_2.

At the experiments starting from serial number of Ru15 a quartz rod with 2.5 mm was placed into the quartz inlet tube. It was important when not only Ru, but other fission product model compounds were applied in the charge. The outer surface of quartz rod was convenient for investigations with XRF and SEM methods to clear up the thermochromatograhphic effects. The weighting of rod and inlet tube was made together.

Photographs of the experimental facility and one sampler unit can be seen in Figures 7 and 8, respectively.
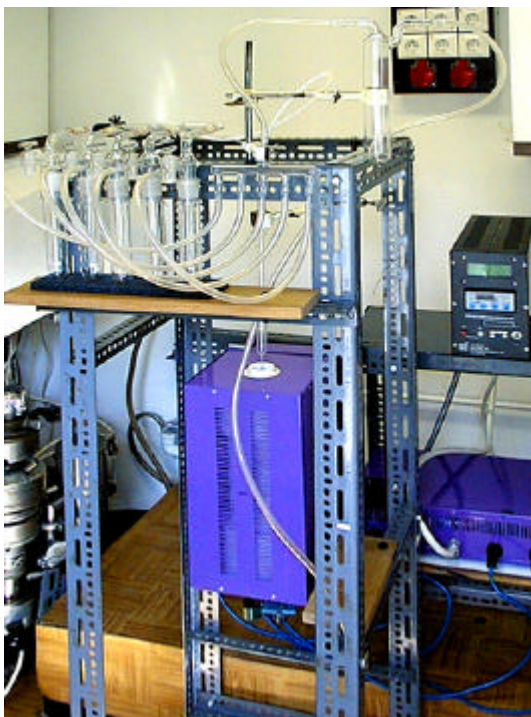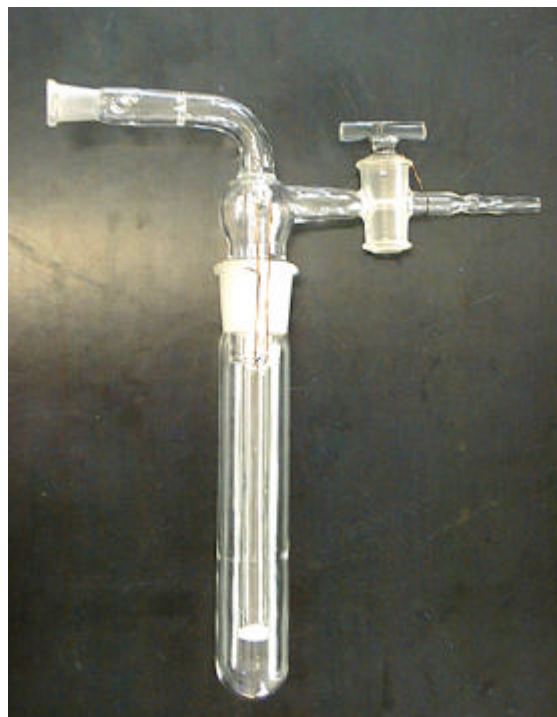

Figure 7. Experimental facility   Figure 8. A single sampler unit No.5

3.2 Chemical analyses

The investigations in frame of the present work needed much chemical analytical activity. The methods have to be prepared to solve the problems. The main tasks were as follows:

3.2.1 Determination of Ru in solutions containing only this element as metallic component,

3.2.2 Investigation of elements on collectors and filters,

3.2.3 Measurement of precipitations on the gas outlet tubes.

Mainly the methods of spectrophotometry, scanning electron microscopy (SEM) together with energy dispersive X-ray analysis (EDX) and X-ray fluorescence (XRF) have been used. These methods are fairly productive to investigate numerous samples in frame of our manpower.

3.2.1 Determination of ruthenium in solutions containing only Ru as metallic element

As mentioned before the RuO_4 was absorbed in 1 n HCl as $RuCl_3.nH_2O$. (The value of n is 3 at crystallic form of this compound; the water is bounded to the Ru atom as complex.) Other then Ru metallic or amphoter element cannot go through the ambient temperature tubing. The absorption vessels contained 30 ml acid solution. Many experiments has been made to find the most advantageous chemical form for the spectrophotometry suggested in the literature. The form of Na-ruthenat [14], complexes with NaSCN [15], 1,10-fenantrolin [16] and rubeanic acid has been investigated. The complexes were not stable in time and the preparation was time consumable. The determination of Ru in about 100 samples in frame of the present work a simple sample preparation has advantage. The best method proved to use the solution of absorber without any pre-treatment.

The determinations were performed by a MOM Spektromom 195D UV-VIS instrument using Suprasil cells with 1 cm length. In Figure 9 the absorbance (A=-lg(Transmission)) is shown in function of wavelength. for absorber solutions of Ru12 experiment 1st and 5th samples, moreover a reference solution prepared from crystallic $RuCl_3.nH_2O$ compound. The maximum values are appeared at 452 nm at all the three cases. It indicate the same chemical form for the Ru at all cases.
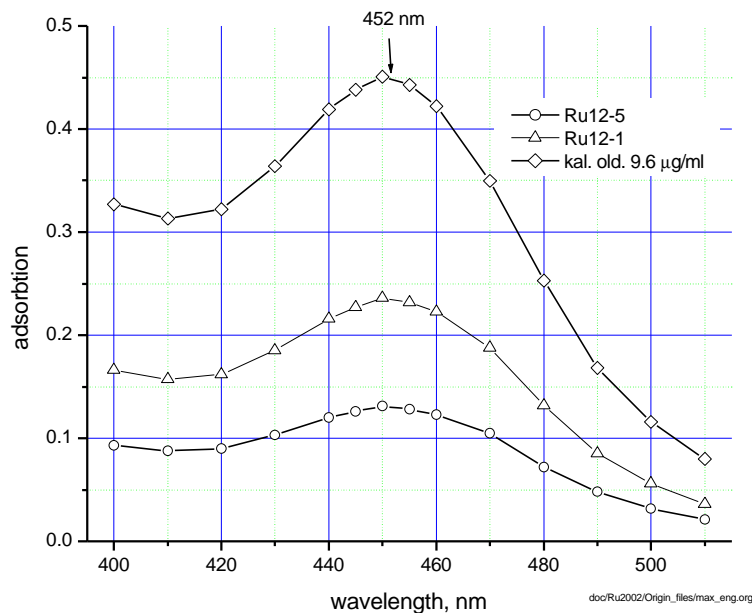
Figure 9. Light adsorption in function of wavelength of $RuCl_3.nH_2O$ in 1 n HCl and absorber solutions from Ru12 test.

The calibration of spectrophotometer has been made by solutions of $RuCl_3.nH_2O$ in 1 n HCl containing 2.4, 4.8 and 9.6 µg Ru/ml. The results are plotted in Figure 10. The absorbances were linear with the concentration, indicating the same chemical form at every dilution.

Figure 10. Concentration of Ru in function of absorbance, 452 nm, 1 cm cell length

3.2.2 Investigation of elements on collectors and filters

The samplers shown in chapter 3.1 were containing quartz fibre filters for collecting the aerosols. At tests Ru15 and Ru16 a similar filter was built in just above the reaction chamber unit. They were investigated by XRF and SEM-EDX methods. The XRF resulted average values regarding the elements with higher atomic weights collected. The SEM-EDX showed the particle sizes and elemental composition as well.

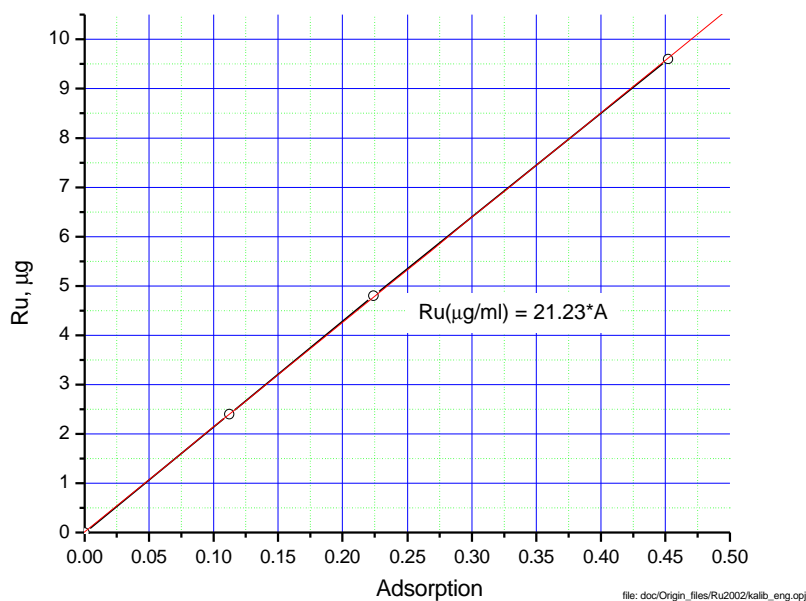The investigations of quartz fiber filters from the inlet tube of samplers gave only poor results. Some aerosol particles were found. They were too far from the reaction chamber outlet, the aerosols were deposited on the tube walls. The filters from the top of reaction chamber quartz tube resulted more useful data.

The *XRF investigations* were made by a Siemens Kristalloflex X-ray fluorescence equipment. It was used in a secondary target mode for the analysis of quartz filters and with microcapillary at the axial distribution investigations of quartz rods. In both case the X-ray tube had a silver cathode, at the secondary target mode the secondary target was silver as well. The X-ray tube was used with 50 kV high voltage and 30 mA current. The Ru, Zr and Mo were measured from the K lines, the Cs from L line. The microcapillary source had an 0.1 mm diameter exciting ray, but the measurements were made by 1 mm steps along the rods. The emitted characteristic X-rays were detected by a Si(Li) semiconductor detector. The signal was collected by computer controlled multichannel analyzer and evaluated by AXIL code.

Scanning electron microscopic (SEM) method was used for the investigations of precipitations on quartz rods from decreasing temperature area of reaction chamber and on aerosol collectors from sampler inlet tubes, as received after the experiments. The quartz fiber filters were coated with a thin carbon layer to prevent from electrostatic charge on their surfaces. The instruments applied were:
- Philips SEM 505 scanning electron microscope, usually with 20 or 25 kV accelerating voltage and a few mA electron current, in backscattered electron image (BEI) mode,
- EDX detector type LINK AN 10/55S,
- EDX detector with thin window made by firm Oxford.

3.2.3 Measurement of precipitations in the gas outlet tubes.

As it was mentioned earlier in the decreasing temperature part of reaction chamber RuO_2 is precipitated as a result of

$$RuO_3 \leftrightarrow RuO_2 + 1/2\, O_2 \qquad\qquad\qquad (4)$$

and

$$RuO_4 \leftrightarrow RuO_2 + O_2 \qquad\qquad\qquad\qquad (5)$$

chemical reactions. In the first series of reactions only Ru was used in the charge as a volatile component in hot air. In these cases the elemental analyses of precipitations were not necessary, their mass, characteristic colour and crystal structure proved without doubts, that it was RuO_2 .

Starting from test No. Ru15 not only ruthenium, but other fission products were mixed into the charge. Quartz rods applied in the inlet tube in these experiments, for their surfaces could be investigated with XRF and SEM-EDX methods. In the first case it was determined, that the precipitations on the inlet tube and quartz rod were in the same height range and their morphology was also the same. The elemental analysis along the rod indicated the relative amount of precipitated volatile components, showing the thermochromatographic effect. The results are discussed in the next chapter.

4. RESULTS AND INTERPRETATIONS

4.1 Summary of experiments

In the frame of the present work 19 high temperature experiments were carried out as summarized in Table I. Our intention was to make a systematic approach starting from simple to complex systems to clear up the effect of the different parameters. An important goal was to clear up the processes going on at the tests with different chemical composition. The columns in the Tables are the followings:

Sample   identification sign of the experiment in RuX-Y form, where X is the serial number of test, Y is the serial number of samples collected in one test. The numbers are growing with the time of test and sampling.

Ru(in)   the mass of Ru powder in mg used for the experiment. In these columns are given other parameters used at the given test,
  - without any sign – dry air, Ru powder in 1 g ZrO_2 matrix,
  - "steam" – 5w% steam in the flowing air,
  - "FP" – other fission product elements in 1 g ZrO_2 matrix as given in Table II.

Temp.   temperature in the reaction area, [°C]

Ru   mass of Ru absorbed in gas sampler 1 n HCl, [µg],

dV/dt   air flowrate at 25 °C temperature, [ml/min]

Time   the sampling time of given sample, [minutes]

V(air)   the total volume of gas(air) flowed through the reaction chamber during the given sampling [litre] (25°C),

Pp(RuO$_4$)   average partial pressure of RuO_4 in air flowing through the sampler 1 nHCl during the sampling time, calculated from the amount of absorbed Ru mass and air volume, [bar],

Eq.temp.   the temperature, when the given Pp(RuO$_4$) value is resulted in equilibrium of $RuO_4 \leftrightarrow RuO_4 + O_2$ reaction, according to the Figure 2 , [°C]

Precip.   the ratio of Ru deposited in the inlet quartz tube related to the Ru(in) [%]. At Ru15-Ru19 other FP compounds are deposited as well, the values are not significant.

Table I

Results of ruthenium experiments (Ru1-Ru19)

Sample	Ru (in.) mg	Temp. °C	Ru μg	dV/dt ml/min	Time min	V(air.) litre	Pp(RuO$_4$) bar	Eq. temp. °C	Precip. %
Ru1-2	5.71	1100	9.6	60	150	9.0	2.63E-07	612.2	
Ru1-3			22.4	60	180	10.8	5.11E-07	652.9	
Ru2-1	6.43	1100	3.2	60	360	21.6			82-89
Ru2-2			0						
Ru3-1	26.3	1100	8.3	150	120	18.0	1.14E-07	565.6	77.5
Ru3-2			45	185	120	22.2	5.00E-07	651.5	
Ru3-3			42	176	120	21.2	4.88E-07	650.0	
Ru3-4			3.8	141	63	8.9	1.05E-07	561.6	
Ru4-1	6.4	1100	68.5	171	120	20.6	8.20E-07	684.2	
Ru4-2			47.4	171	120	20.6	5.67E-07	659.7	
Ru4-3			63.4	171	120	20.6	7.59E-07	679.0	
Ru4-4			60.8	171	120	20.6	7.28E-07	676.1	
Ru5-1	6.20	1100	84	300	30	9.0	2.30E-06	760.5	
Ru5-2			54	300	30	9.0	1.48E-06	726.3	
Ru5-3			84	300	60	18.0	1.15E-06	707.9	
Ru5-4			177	300	120	36.0	1.21E-06	711.7	
Ru5-5			122	300	120	36.0	8.35E-07	685.5	84
Ru6-1	6	1000	58	171	123	21.1	6.77E-07	671.3	49
Ru6-2			43	171	120	20.6	5.15E-07	653.4	
Ru6-3			33.3	171	120	20.6	3.99E-07	637.3	
Ru6-4			28.8	171	120	20.6	3.45E-07	628.4	
Ru7-1	6.01	1100	43.5	171	60	10.3	1.04E-06	700.9	
Ru7-2			35.2	171	60	10.3	8.43E-07	686.1	
Ru7-3	SS plate		83.8	171	120	20.6	1.00E-06	698.3	
Ru7-4			81.3	171	120	20.6	9.73E-07	696.1	
Ru8-1	6.2	1200	59.5	171	30	5.1	2.85E-06	777.9	87
Ru8-2			113.0	171	60	10.3	2.71E-06	773.6	
Ru8-3			126.0	171	60	10.3	3.02E-06	782.6	
Ru8-4			137.0	171	60	10.3	3.28E-06	789.6	
Ru8-5			198.0	171	60	10.3	4.74E-06	821.7	
Ru9-1	5.5	1100	111	171	120	20.6	1.33E-06	718.5	75
Ru9-2	(steam)		140	171	120	20.6	1.68E-06	735.8	
Ru9-3			148	171	120	20.6	1.77E-06	740.1	
Ru9-4			112	171	120	20.6	1.34E-06	719.1	
Ru10-1	6.05	1100	54.4	171	60	10.3	1.30E-06	717.0	95

Ru10-2	air		36.5	171	60	10.3	8.74E-07	688.6	
Ru10-3	+ ZrNb		30	171	74	12.7	5.82E-07	661.4	
Ru10-4			40.3	171	70	12.0	8.27E-07	684.8	
Ru10-5			61.4	171	90	15.4	9.80E-07	696.6	
Ru11-1	argon	1100	0	171	120	20.6			0
Ru11-2	argon+		0	171	120	20.6			0
	steam								
Ru12-1	5.85	1100	150	171	60	10.3	3.59E-06	797	60.6
Ru12-2			94.1	171	60	10.3	2.25E-06	759	
Ru12-3	steam		113	171	120	20.6	1.35E-06	720	
Ru12-4			103	171	120	20.6	1.23E-06	713	
Ru12-5			77.1	171	120	20.6	9.23E-07	692	
Ru13-1	6.00	1100	77	171	30	5.1	3.69E-06	800	72.5
Ru13-2			58	171	30	5.1	2.78E-06	776	17.7
Ru13-3			0	171	30	5.1			0
Ru14-1	5.25	1100	154	171	30	5.1	7.37E-06	863	68
Ru14-2	filter		17.3	171	30	5.1	8.28E-07	685	7.3
Ru14-3			0	171	30	5.1			
Ru14-4			0	171	30	5.1			
Ru15-1	5	1100	0.6	171	32	5.5	2.69E-08	496	ca 110
Ru15-2	+ other		6	171	32	5.5	2.69E-07	614	ca 9
Ru15-3	FP+steam		14	171	32	5.5	6.28E-07	666	
Ru15-4			0	171	60	10.3			
Ru16-1	5	1100	0	171	30	5.1	0.00E+00		ca 110
Ru16-2	+ other		45	171	30	5.1	2.15E-06	755	0
Ru16-3	FP		26	171	30	5.1	1.25E-06	714	ca 7
Ru16-4			48	171	60	10.3	1.15E-06	708	0
Ru17-1	5	1100	0	171	30	5.1	0.00E+00		ca100
Ru17-2	+other		1.3	171	30	5.1	6.23E-08	535	
Ru17-3	FP+steam		6.3	171	30	5.1	3.02E-07	620	
Ru17-4			82.3	171	120	20.6	9.85E-07	697	
Ru17-5			180	171	195	33.4	1.33E-06	718	
Ru18-1	5	1100	24	171	120	20.6	2.87E-07	617	>100
Ru18-2	+other		163	171	60	10.3	3.90E-06	805	
Ru18-3	FP+steam		175	171	60	10.3	4.19E-06	811	
Ru18-4	+UO$_2$		184	171	60	10.3	4.41E-06	815	
Ru18-5			230	171	120	20.6	2.75E-06	775	
Ru19-1	5	1100	96	171	60	10.3	2.30E-06	760	>100
Ru19-2	+ other		190	171	60	10.3	4.55E-06	818	
Ru19-3	FP		193	171	60	10.3	4.62E-06	819	
Ru19-4	+UO$_2$		185	171	60	10.3	4.43E-06	816	
Ru19-5			132	171	60	10.3	3.16E-06	787	

4.2 Ru powder in ZrO$_2$ matrix (Ru1 - Ru14)

4.2.1 Pre-experiments (Ru1-Ru3)

The aim of the first three experiments was to check the operability of the high temperature facility and to some get preliminary information on the evaporation and escape of Ru. However some important behaviour of Ru and its oxides have been recognized.

- The Ru powder escaped with the high temperature air from the ZrO$_2$ matrix during the time calculated from literature data. No Ru has been found in the ZrO$_2$ matrix with XRF or optical microscopy.
- A large part of Ru has been precipitated as RuO$_2$ from the air stream at the decreasing temperature area of outlet tube in form of characteristic deep blue crystals, (CVD - chemical vapor deposition).
- The dissolution of deposited RuO$_2$ could not made with acceptable methods, for this reason weighting by chemical analytical balance was applied to the inlet quartz tube in the decreasing temperature part. (The typical mass of precipitation was about 6-8 mg.)
- The RuO$_4$ - RuO$_2$ equilibrium did not follow the law given in Chapter 3, but the partial pressure of RuO$_4$ even at room temperature remained at a high value $\sim(1\div4)*10^{-6}$ bar, corresponding to that of 500-700 °C.
- The efficiency of gas absorber with 1 n HCl was perfect.
- A slight blue coloured veil appeared on the quartz fiber filter in the inlet of sampler but particles could not be seen by SEM. The size of particles was under the resolution power of SEM. After 2-3 weeks the colour disappeared, the air oxidized the colloidal RuO$_2$ to volatile RuO$_4$. The mass of ruthenium on the filters measured by XRF were the following:

Sample	Ru(μg)	Sample	Ru(μg)	Sample	Ru(μg)
Ru1-1	18	Ru2-1	26	Ru12-1	11
Ru1-2	29	Ru2-2	20	Ru12-2	18
Ru1-3	38	Ru2-4	13		

These quantities are lower then 1% of the initial ruthenium mass in the charge.

4.2.2 Influence of air streaming rate (Ru1, Ru4, Ru5)

In these experiments all parameters were the same except the gas flowrate. The final equilibrium temperature was calculated on the same way as earlier. The results of the first samplings were not taken into consideration, because at the beginning the crystalic deposition were probably less and its catalytic effect for the equilibrium process was not strong enough, that is why these RuO$_4$ partial pressures were higher. The equilibrium temperatures (t(eq.)) were resulted as followings:

Ru1(3)   60 ml/min   t(eq.) = 652 °C

Ru4(3,4)   171 ml/min   t(eq.) = 677 °C
Ru5(3,4)   300 ml/min   t(eq.) = 709 °C

The reason of the rising temperature can be attributed to the fact, that the rate of chemical process leading to equilibrium is at the time range, until the gas is streaming through the decreasing temperature zone and at higher flow rate higher partial pressure of ruthenium tetroxide remain in the air (resulting higher equilibrium temperature).

4.2.3 Influence of reaction chamber temperature (Ru5, Ru6, Ru8)

In these experiments the influence of reaction chamber temperature has been studied. At Ru6, Ru5 and Ru8 the temperatures were 1000, 1100 and 1200 °C , respectively. The differences in the escaping RuO_4 partial pressures were larger than it was expected with 630, 700 and 780 °C equilibrium temperatures. It indicated again, that from the larger RuO_4 partial pressures coming from the reaction chamber a larger part remained back because of the not perfect chemical equilibrium with decreasing temperature.

4.2.4 Influence Zr1%Nb cladding material (Ru10)

Pieces with some mm dimensions of original Zr1%Nb cladding material have been given to the ZrO_2 - Ru powder mixture of 0.2 g weight to reflect the ratio of fuel element. It did not influence the release of ruthenium. This is not a surprising result, because at 1100°C and the high air stream rate the cladding metal has been oxidized in some minutes, or at least a thick oxide layer has been formed on the metal surface. In a real accidental situation a similar situation can be expected. At the time of air ingress the cladding is certainly strongly oxidized.

4.2.5 Stainless steel in the decreasing temperature area (Ru7)

The experts of PHEBUS FP program suggested this test to get information regarding the influence of stainless steel surfaces. The question was the influence of SS surfaces on the release of Ru. A 0.5 mm thick 170x2.6 mm SS plate has been placed into the quartz inlet tube of decreasing temperature area. The RuO_2 precipitation formed on the SS plate was at the same height interval as in the quartz inlet tube surface. Even the morphology of precipitation was the same on SS as on quartz. The mass of precipitation cannot be weighed, because of the oxidation of SS resulted a substantial mass increase over the RuO_2.

4.2.6 Influence of steam (Ru9, Ru12)

Using air with steam content (ca 0.05 bar steam) the freezing of the RuO_4 - RuO_2 equilibrium happened at ~1.3-1.8 µbar RuO_4 partial pressure, wich corresponds to temperatures higher for 20 °C than in dry air 720-740°C. The partial pressure was calculated on the basis of Ru mass collected in the gas samplers. In this test less Ru precipitated in the

inlet tube and some more in the tube system going to the sampler unit. The steam delayed the process leading to the equilibrium.

4.2.7 Time dependence of Ru-dioxide precipitation (Ru13, Ru14)

In these experiments the quartz inlet tubes were changed together with the absorber units, at about every 30 minutes. The weight increase showed the amount of deposits in time. Supposing that during the first 30 minutes the air was saturated with ruthenium tri- and tetroxides, the deposit on the second 30 minutes gave a time until saturated air was coming. This assumption resulted Ru escape time for Ru13 37.3 minutes, for Ru14 33.2 minutes. The air volume streaming through was 6378 and 5677 ml, respectively. The charged Ru was 6.00 and 5.25 mg. The average total RuO_3 and RuO_4 partial pressures were $2.48*10^{-4}$ and $2.43*10^{-4}$ bars for Ru13 and Ru14. The value calculated from equation of [18], given in Chapter 2 in equations of (i) and (ii) is $2.43*10^{-4}$ bar. These results were showing that the
- air leaving the reaction chamber is saturated for Ru oxides, until Ru powder is in the ZrO_2 matrix,
- the applied equations are correct.

In Ru14 experiment a quartz filter was just at the top of reaction chamber outlet tube. The difference in Ru content of absorber liquids compared to that of Ru13 did not indicate that a significant amount of Ru would be carried away by aerosols.

In the Ru13 and Ru14 experiments the quartz inlet tubes were changed at the same time as absorbers. In the 3rd and 4th absorber solutions there were no Ru. It proved, that the later Ru escapes were coming from the deposited RuO_2 by re-evaporation into the high temperature air.

4.3 Ru powder in ZrO$_2$ matrix together with other FPs (Ru15, Ru16, Ru17)

In these experiments the charge in reaction chamber contained other fission products formed in a fuel at 44 MWd/kgU,[8] burnup. No UO$_2$ was added to the initial powder. The composition of the mixture is given in Table II. It did not contain all the fission products being in the burned up fuel, some of them were replaced by others with similar chemical behaviour, but the amount is representative.

Table II.
Composition of fission product model charge

Species	Quantity for one charge	
	mg	μmol
Cs$_2$CO$_3$	4.12	25.3
CsI	0.97	3.7
BaCO$_3$	4.43	22.4
Ru	5.06	50.1
Mo	3.79	39.5
Se	0.088	1.1
Sn	0.094	0.79
Ag	0.079	0.73
Sb	0.039	0.32
Cd	0.153	1.36
Te	0.738	5.78
Nd$_2$O$_3$	11.32	67.3
CeO$_2$	4.1	28.3
ZrO$_2$	5.38+1000*	44.1+8130*
	(* 1 g ZrO$_2$ matrix)	

In Ru15 and Ru16 tests the inlet quartz tubes were changed together with the samplers, at Ru17 the same tube was used during the experiment. In Ru15 and Ru17 wet air, in Ru16 dry air was used.

The most significant difference from the earlier experiments – where the charge was rutenium powder in zirconium-dioxide – that the release of Ru started in the beginning of the experiments with lower intensity and with certain delay. The weight increase did not resulted acceptable results because of some FP elements were also evaporated. XRF and SEM-EDX investigations were made at the next samples:
- on quartz rods from inlet tubes:
    - with XRF vertical elemental distribution of Ru15 and Ru16 test,
    - with SEM-EDX of rod from Ru16; morphology of deposition, particle elemental distribution,
- on filter above the reaction chamber, Ru15, morphology of deposition, particle elemental distribution, SEM-EDX
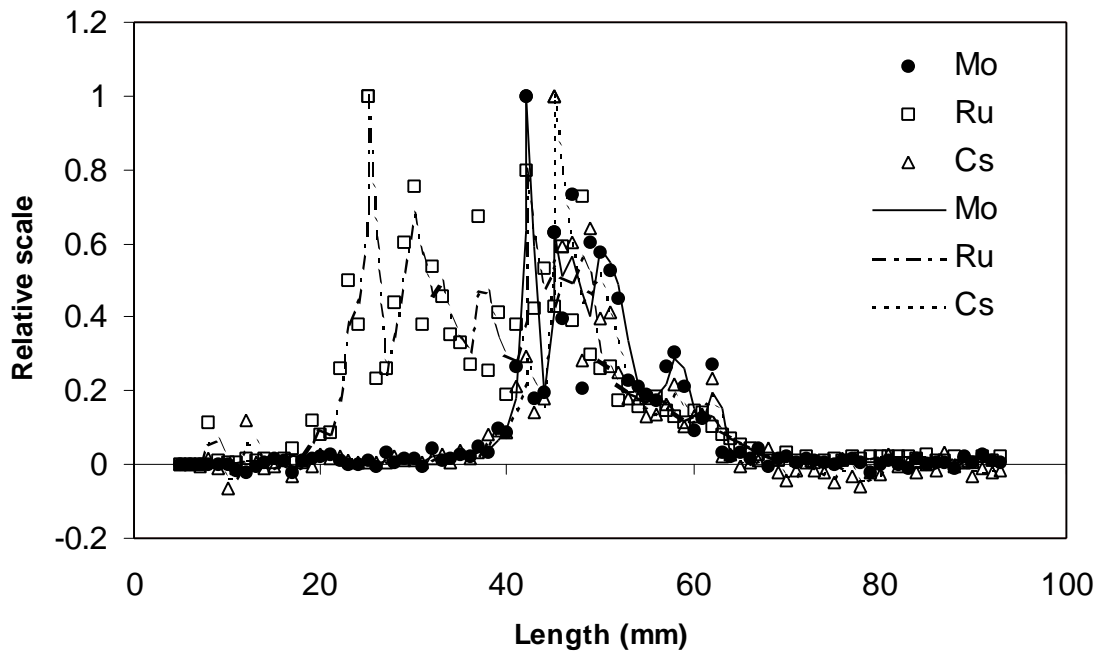- on Si and Ni plates and filters from inlet tube of samplers, SEM-EDX.

Figure 11. Deposits in quartz rod in case of FP-s in ZrO_2 matrix.
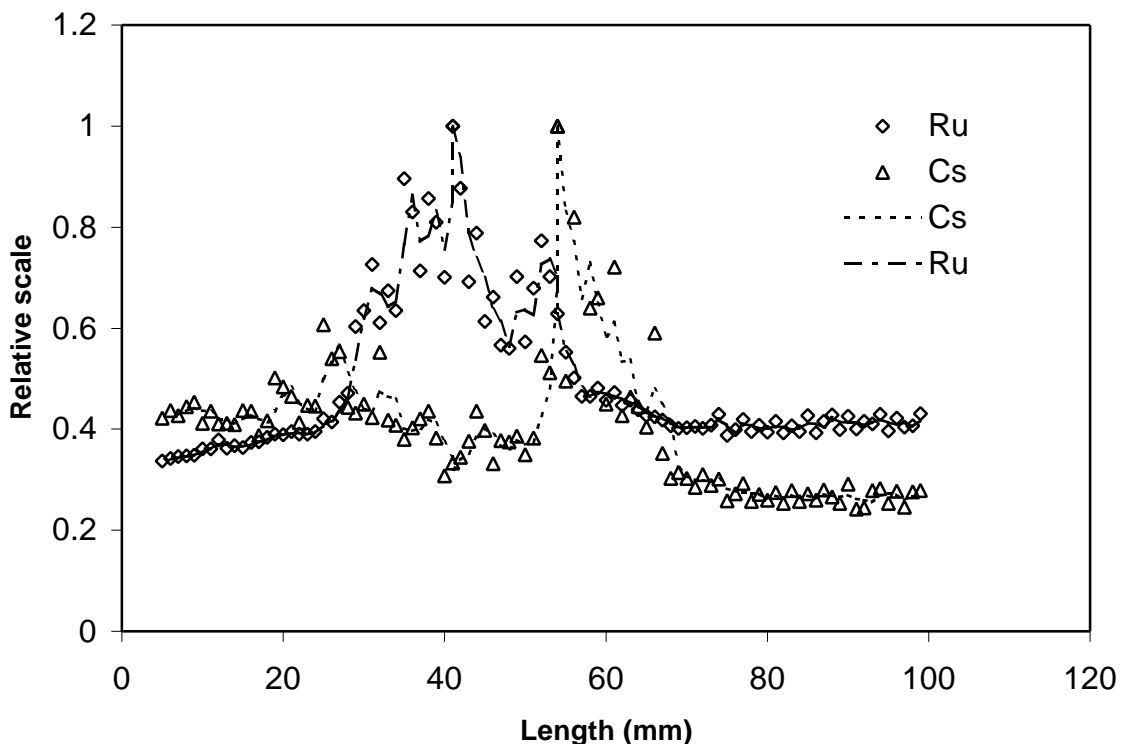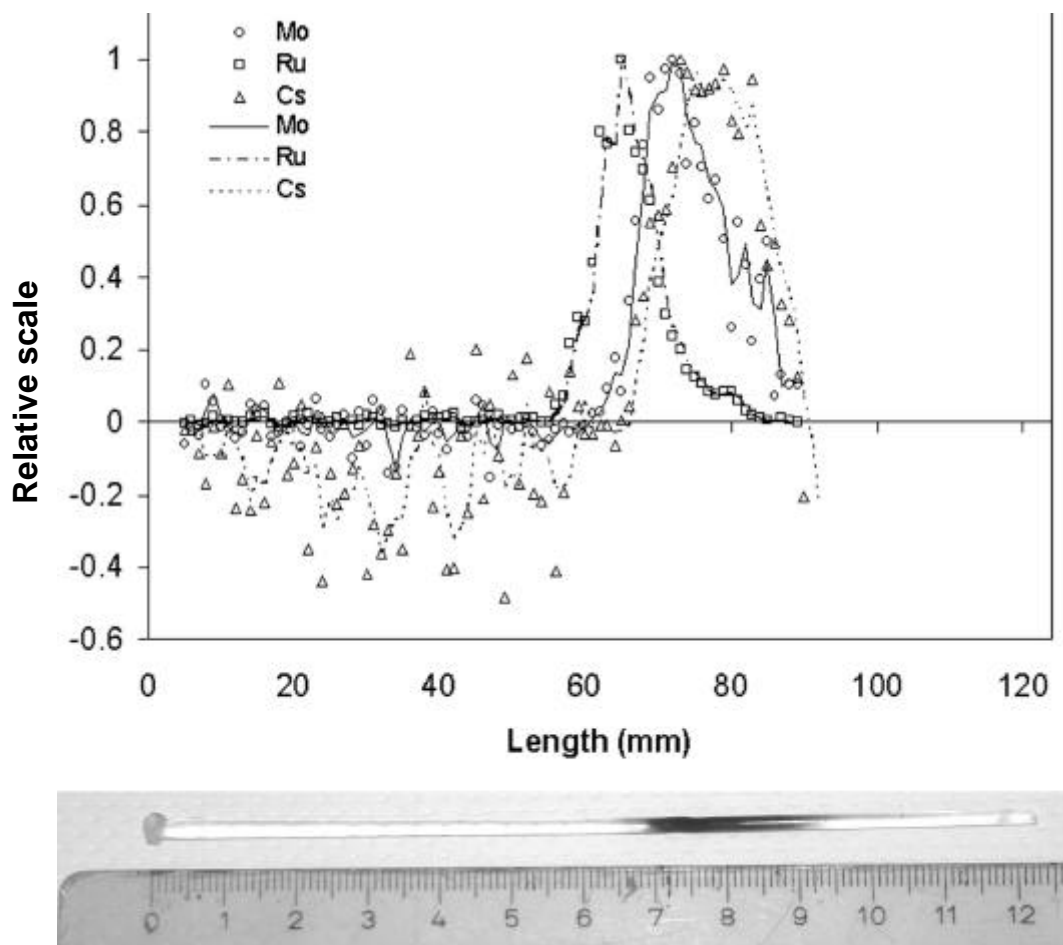(Sample Ru15-1, wet air, 1100°C, XRF capillary method)

Figure 12. Deposits in quartz rod in case of FP-s in ZrO_2 matrix.
(Sample Ru16-1, dry air, 1100°C, XRF capillary method)

The axial distribution of elements on the vertical quartz rods made by XRF microcapillary method showed the thermochromatographic effect clearly. The results

regarding the Ru15-1 rod sample are shown in Figure 11. (At the Figures 11/13 left sides are always the high temperature, rights are the low temperature part, left were in the furnace, the rights were at the top above the furnace near to ambient temperature.) The results are relative values at every element, 1 is the highest intensity.

At sample Ru15-1 the Ru (RuO_2) was enriched at two sites, at the lower height (higher temperature part) only ruthenium, at the lower temperature part Cs and Mo appeared as well. The maximum values of all the three elements are at the same site. Presumable ruthenates were formed, otherwise the thermochromatographic effect would separate them. At sample Ru15-2 (no figure given) only Ru appeared at the same height as at Ru15-1, Cs and Mo were under the analytical sensitivity limit.

The Ru16-1 sample (shown in Figure 12) is from a similar experiment, but with dry air. In this case Mo was not found, the Cs appeared at the highest part of Ru deposit. The second maximum of Ru is not entirely separated, the slower decreasing of Ru curve indicate it.

At the Ru16-2 sample (Figure 13) both the Mo and Cs showed a maximum in appearance, together with a small, but definite Ru maximum. The coincidence of Ru second maximum and the Cs is more definite. It seems that the escape of Mo is faster in case of wet air.

Figure 13. Deposits in quartz rod in case of FP-s in ZrO_2 matrix.

(Sample Ru16-2, dry air, 1100°C, XRF capillary method)

We performed direct electron beam studies both on quartz rods having deposits on their surfaces and on samples collected by aerosol sample collectors. We sputtered a thin carbon layer on quartz fiber filters due to their electric charging. The following instruments were applied:

- Philips SEM 505 scanning electron microscope (SEM) working at 20 or 25 kV and using a few nanoamper beam current. Mostly we made backscattered electron images (BEI).
- LINK AN 10/55 S type electron beam microanalyser (EDX).
- Oxford EDX using thin window suitable for detecting light elements such as oxygen, carbon and boron.

The aim of our SEM studies was twofold:
1. To know the *morphology of deposits* present on the inner quartz rod No. Ru16-1.
2. To reveal the nature of deposits and aerosols formed at low temperature in experiment No. Ru15. Deposits and aerosols were collected on quartz fibre filters and on aerosol collectors. (Both in experiment No. Ru15 and in Ru16 we used ZrO_2 matrix and a mixture containing the fission product components as described earlier. In the preceding experiment wet air, while in the latter dry air was applied.)

Five pieces of the rod No. Ru-1 were cut after the XRF measurements. We mounted the rod pieces on SEM sample holders covered by adhesive carbon tape. We labeled the samples in a way that the sample nearest to the outside space got No. 1, then the numbers increased by proceeding to the direction of the oven. We mounted the samples in such a way, that their upper ends were closer to the outside space, while their lower ends to the oven. We made small magnification (45-times) SEM images from the two ends and from the middle part of the quartz rods. This magnification was appropriate to reveal the degree of deposition. For samples No. 1 and 3 we made images even from more sample regions. At the ends and at the middle parts of the samples we always made EDX analysis at magnification of 300-times, which corresponded to about 1 mm^2 area. We also examined sample details having brighter contrast, i.e. higher atomic number of elements, than their neighbourhood, and made images with higher magnification.

Rod piece No. 1: Small magnification image series of this sample is shown in the upper part of Figure 14. It can be seen that only small amount of deposit formed on the part nearest to the outside space, while its quantity increased by proceeding to the direction of the oven. EDX analysis of the rod end directed to outside has shown the presence of Te, Ru, Mo and small amounts of Cs. By advancing to the direction of the oven, we could find relatively large aggregates of grains on the surface of the rod, which had bright contrast. Their EDX analysis revealed that they were enriched in Te. Besides Te, they contained less amounts of Mo and Ru. In some deposited grains with bright contrast, we detected Cs beside Te, further smaller amounts of Ru and Mo. The average EDX analysis of the rod end nearest to the oven has shown the presence of Te, Ru and Mo. It is worth to look at the shape of some deposited grains: the ones richest in Te were large crystals with regular forms. Their length was several tens, even hundred μm, while their width varied between 10 and 30 μm. There were deposited grains with rim parts: the components of the rim: Te, Mo, and Ru, probably small amounts of

Cd, however there were details of the rimmed structure, where we could detect Zr and Cs, too. Ruthenium enriched mostly at the rims of the honeycomb-structure, besides we detected lower amounts of Te and Cs. Typical deposited grains can be seen in Figure 15.

Rod piece No. 2: The small magnification image series of this rod part can be seen in the lower part of Figure 14. These images have shown dense deposition on the surface of the rod piece. The EDX analysis of various areas revealed the presence of Ru, Cs and Mo, in a few cases also the presence of Cs. By moving to the direction of the oven, Te was rarely present. Deposits were mostly Ru-oxide accompanied by Mo and Cs.
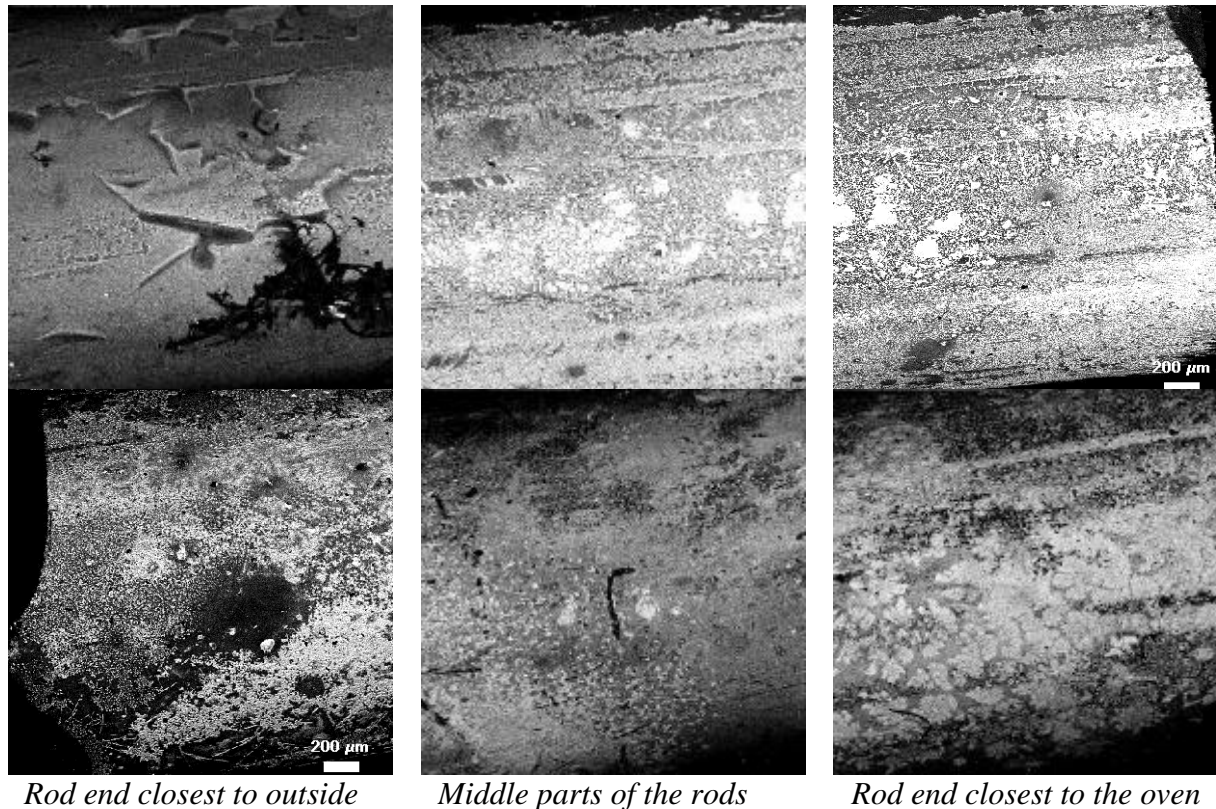
| *Rod end closest to outside* | *Middle parts of the rods* | *Rod end closest to the oven* |

Figure 14: Digital BE images for rod No. 1 (upper images) and for rod No. 2 (lower images) with 45 times of magnification
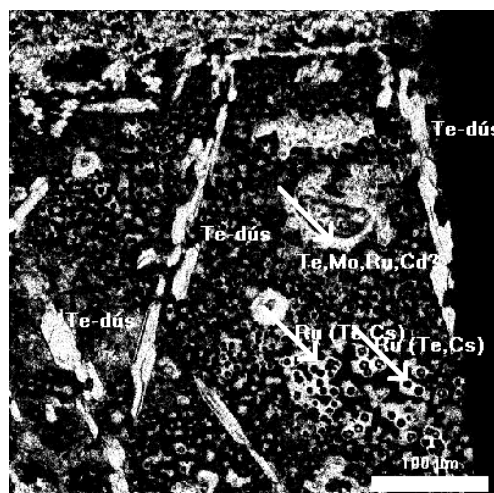
Figure 15: Deposits typical for rod No. 1 on BE image with 220 times of magnification

Rod piece No. 3: The small magnification image series can be seen in the upper part of Figure 16. This rod piece was also densely deposited, among the deposited grains there were larger sized irregular and globular ones, too. The average EDX analysis has shown the presence of Ru, lower amounts of Cs and Mo. The ratio of the Cs and Mo depended on the abundance of deposited grains - having brighter contrast (mostly enriched in Cs) – in a given analysed area. One example for such Cs-rich grain is illustrated in Figure 17.

Rod piece No. 4: The small magnification image series can be seen in the lower part of Figure 16. The average EDX analysis of the rod part nearest to the outside space has revealed the presence of large amounts of Ru and low amounts of Cs and Mo. The two latter elements originated from deposited grains having brighter contrast than the sample surface. Example for such grains can be seen in Figure 18. (on the left hand side). Ru enriched in rectangular crystals, while sample details enriched in Cs were generally aggregates of grains (see the lower image of Figure 18.). Probably grains enriched in Cs and Mo deposited later on the Ru-rich base material. By moving to the direction of the oven, the main component was Ru, apparently there were deposited grains enriched in Cs and Mo, too. At the rims of the honeycomb structure enrichment of Cs could be recognised together with Mo and Ru (inside there was the glass).
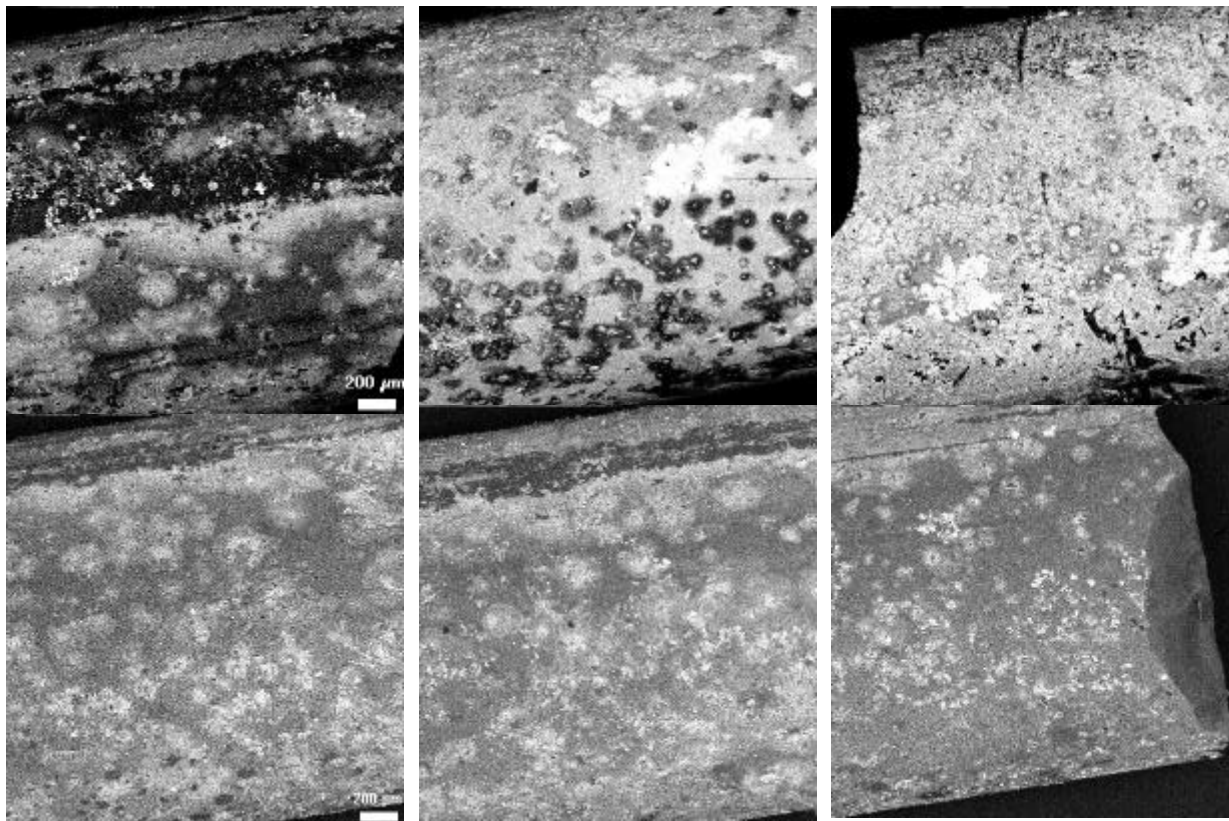
Rod end closest to outside   *Middle parts of the rods*   *Rod end closest to the oven*

Figure 16: Digital BE images for rod No. 3 (upper images) and for rod No. 4 (lower images) with 45 times of magnification

Rod piece No. 5: The small magnification image series of this sample part is shown in Figure 19. It can be recognised that there was less deposition at the end nearest to the oven, than the one closer to the outside space. The average EDX analysis of rod part closer to the oven has shown low amounts of Cs, Mo and Ru. By moving to outside, the quantity of deposited material increased. More and more amounts of deposited grains could be found with increasing size. Their main component was Ru, besides lower amounts of Cs and Mo could be detected. These latter elements originated from globular or irregular shaped deposited grains. Figure 17 has shown the large scaled base deposition, enriched in Ru, and the nearly globular grains enriched in Cs. In average the main component was again Ru by moving to the direction of the oven; however there were relatively high amounts of grains containing Cs (some of them were situated at the edge part of the rod).

By summarizing the above, it could be stated, that in case of the inside quartz rod, Ru (probably oxide) was the main component at the rod end closer to the oven, it formed large sized deposited grains. Probably Cs and Mo deposited at some regions on it. By moving to outside and getting further from the oven, Te formed relatively large sized grains on the surface of rod piece No. 1.
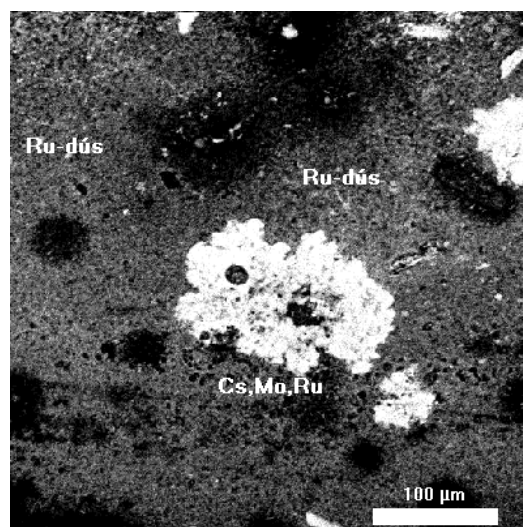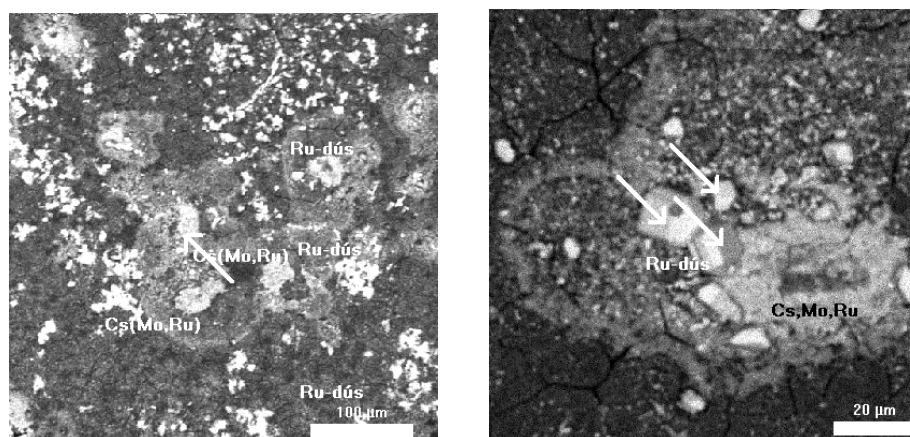

Figure 17: Deposits typical to rod No. 3

Figure 18: Deposits rich in Cs-Mo-Ru and in Ru, respectively on the surface of rod No. 4

Rod end closest to outside   *Middle part of the rod*   *Rod end closest to the oven*
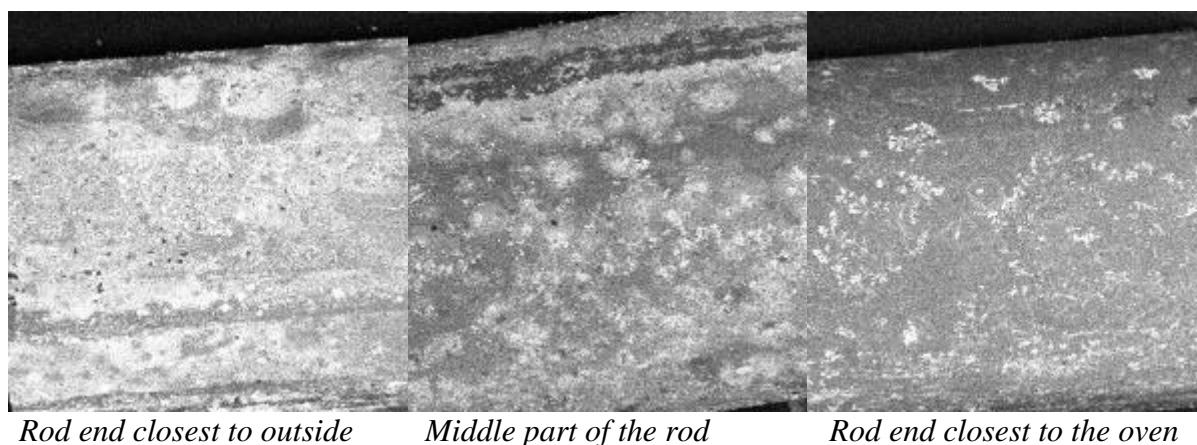
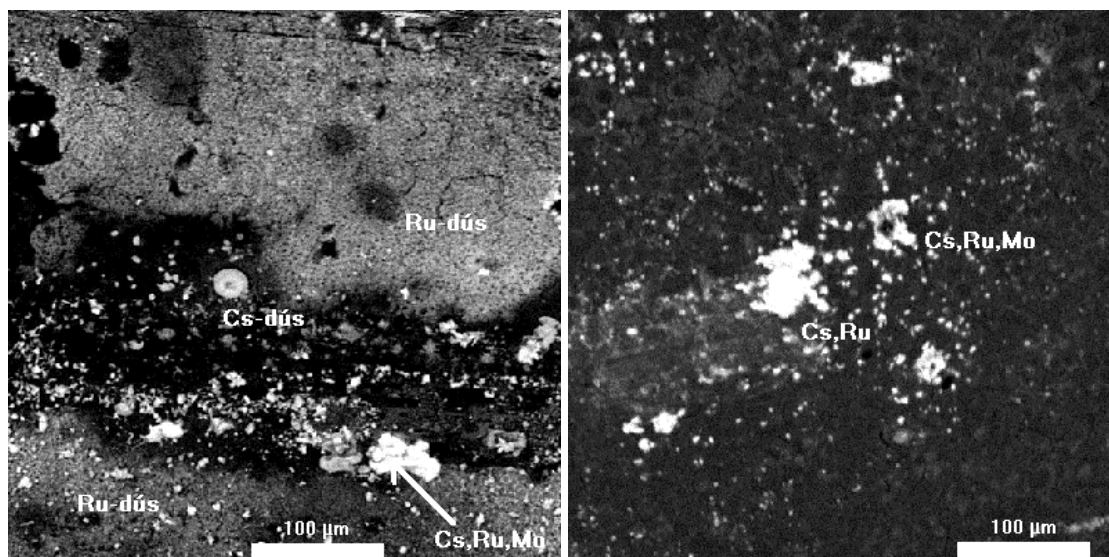Figure 19: Small magnification image series of rod No. 5

Figure 20: Deposits typical to the middle part and to the end closest to the oven for rod No. 5 at 220 times of magnification

In the experiment No. Ru15 we studied quartz fibre filters and aerosol collectors by means of electron beam methods. We examined the following samples:

        Ru15   filter placed above the reaction space

        Ru15-1: 3 samples collected on Ni and Si holders and on quartz filter, respectively.

        Ru15-2: 3 samples collected on Ni and Si holders and on quartz filter, respectively.

        Ru15-3: 3 samples collected on Ni and Si holders and on quartz filter, respectively.

Sample No. Ru15. contained grains collected on quartz filter, while for the other three samples we used three types of holders: nickel sheet, silicon plate and quartz filter, respectively.

SEM study of the surface of Ru15 sample at small magnification has shown that the filter surface was densely covered; there were a lot of grains and aggregates. It is illustrated in Figure 21, which is digital BEI at 500-times of magnification.
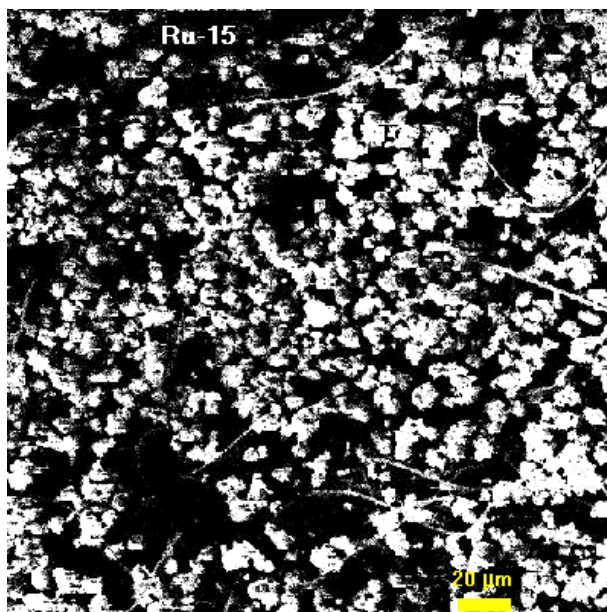

Figure 21: BE image typical for sample No. Ru 15 at 500 times of magnification

Average EDX analysis of the sample has shown that the main component was Zr (oxide), besides Se and Ru could most frequently be detected. Rarely and by analysing individual grains other components: small amounts of Te and Cs, further Nd or Mo could be found, too. Mostly Zr (oxide) was the main component of the individual grains, too. Rarely Ru was the main component, but even in this case lower amounts of Zr and Se could also be detected. Aggregate of grains with such composition is shown on the left side of Figure 22 (digital BEI taken at 1700-times of magnification). The shape of Ru-rich grains was triangle or irregular, while the other grains had generally globular or slightly elongated forms (probably grains formed from aerosol). Such grains are shown in the other digital BEI of Figure 22 taken at 1500-times of magnification. Determination of the elemental composition was done by EDX method.
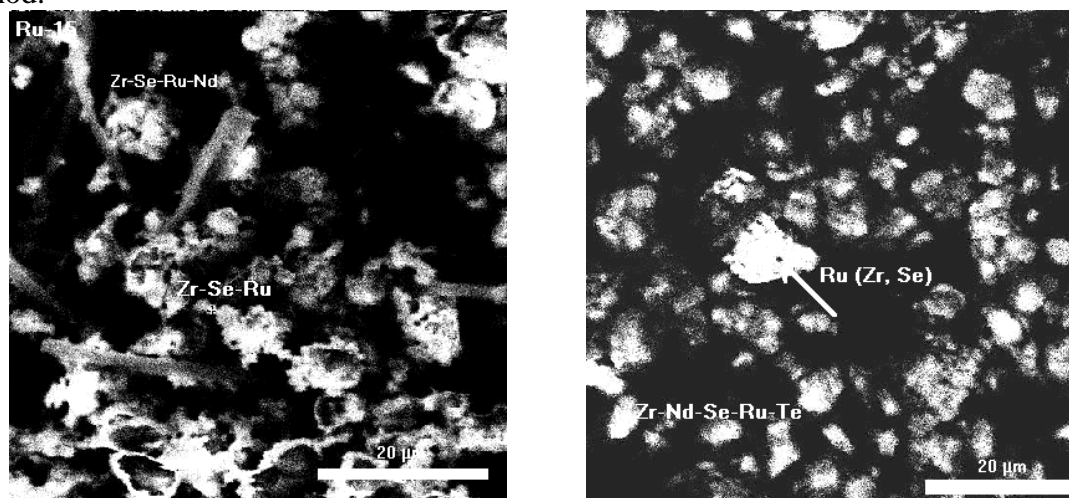

Figure 22: BE images at 1700 and 1500 times of magnification, respectively, for sample No. Ru-15 showing grains with elemental composition characteristic to this sample

In some grains Nd was the second most frequent component following Zr, however lower amounts of Se and Ru could be detected in these grains, too. Rarely small amount of Mo was also found besides Zr, Se, Nd and Ru.

There were various amounts of deposit on samples Ru15-1 at the surfaces of different holders. We found that the degree of deterioration of the sample holders made of various materials varied for the effect of iodine used in the experiment. Traces of degradation caused by iodine were found to be the highest for nickel sample holder: there were a lot of „corrosion" spots and in their neighbourhood small sized grains with globular shape were present. The size of these grains varied between about 1 micrometer and a few micrometers. These grains were arranged mostly in arrays. Such grains are shown on the left hand side image of Figure 23 at 500-times of magnification, while the right hand side image has illustrated splitting inside in corrosion spot. This latter image was taken at magnification of 2800-times. Studies of the elemental composition of the corrosion spots revealed the presence of the following elements: Ni, O, I and small amount of Ru. It has to be mentioned, that identification of Ru is troublesome due to the fact, that the Ru L alpha lines coincide with the K alpha lines of Cl and there was HCl vapour in the experiment. However the presence of oxygen supports the presence of Ru in these spots.
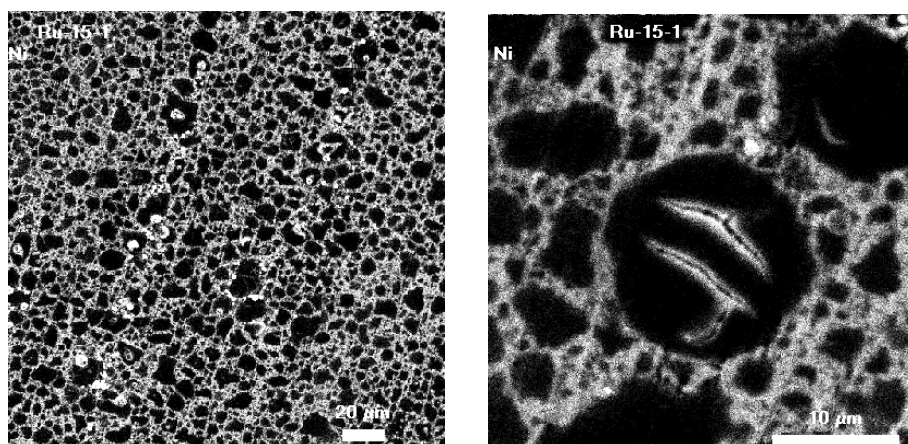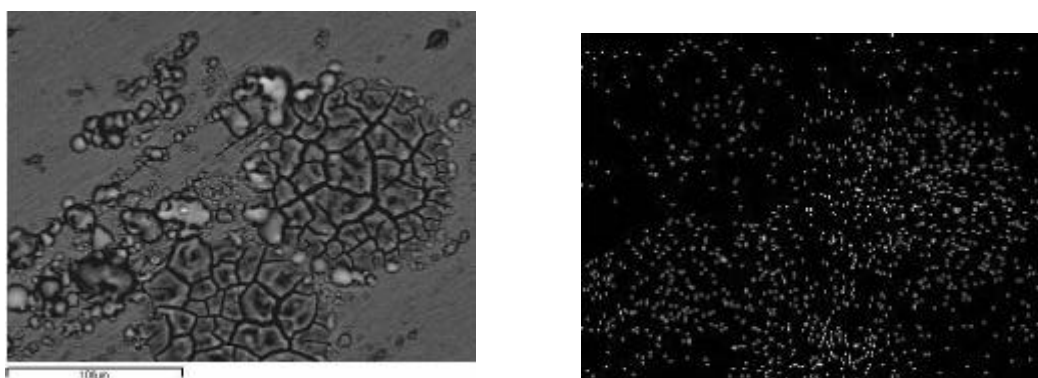

Figure 23: Digital BE images at 500 and 2800-times of magnification for sample exposed to the effect of iodine

Figure 24 has shown BE image and the corresponding X-ray images taken with an Oxford EDX system suitable for detecting light elements. This EDX is attached to an electron microprobe (or wavelength dispersive microanalyser).

BEI   I Lα

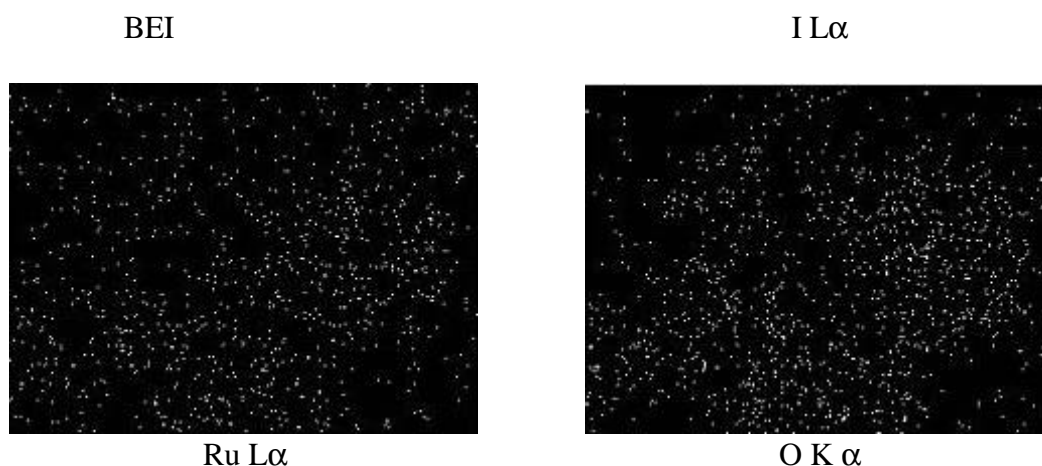Ru Lα   O K α

Figure 24: Digital BE image and the corresponding X-ray images of I, O and Ru
for deposit with I content

It can be seen in the figure that iodine caused not only corrosion spots but it was precipitated in form of aerosol-like particles. In their elemental composition I and low amounts of Ru could be detected (together with some oxygen). Distribution of I corresponded to the morphology of the corrosion deposition.

The Si *holder* was more resistant against the effect of I than the one made of Ni: there were less corrosion spots and they were not so deep, however some grains could be found on its surface. Figure 25 has shown typical BEI at 500-times of magnification from the surface, where less corrosion spots and grains could be found, than for the Ni.
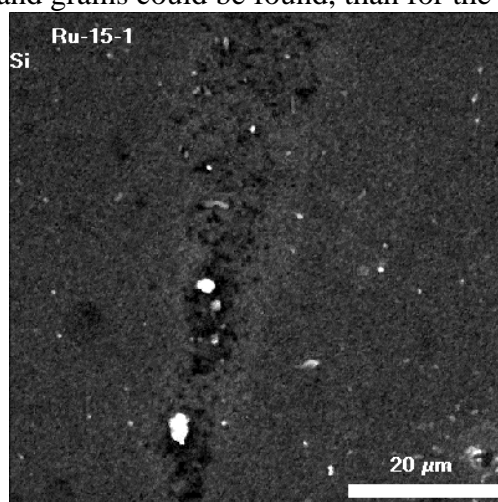

Figure 25: Surface of the Si holder at a digital BE image with 500-times of magnification

The main component of the few grains was I (except for the ones having Si), Ru could not be detected.

Sample collected on quartz filter contained only a few grains. They were mostly Zr-oxide; in some cases we detected also Nd and Ru. The size of the grains was 1.5 – 2 μm. Figure 26 shows typical digital BEI at 900-times of magnification. In this figure we can see Zr-rich grain.
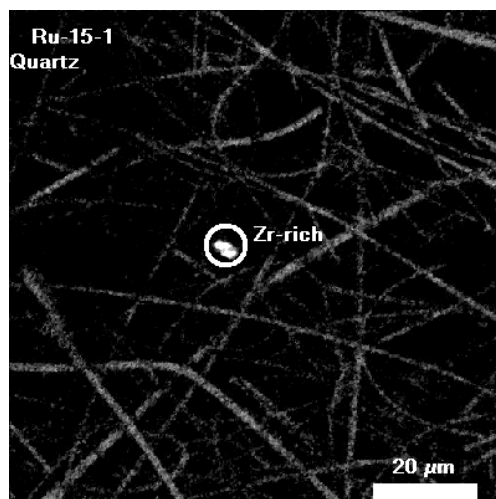
Figure 26: Surface of the quartz filter of sample No. Ru-15-1 on a digital BE image with 900-times of magnification

From samples Ru15-2 the *Ni sample holder* showed the effect of iodine not so strongly than in the other samples. There were less number of corrosion spots and grains with I and probably Ru content. Typical region of the sample can be seen in Figure 27, which was taken at 900-times of magnification.
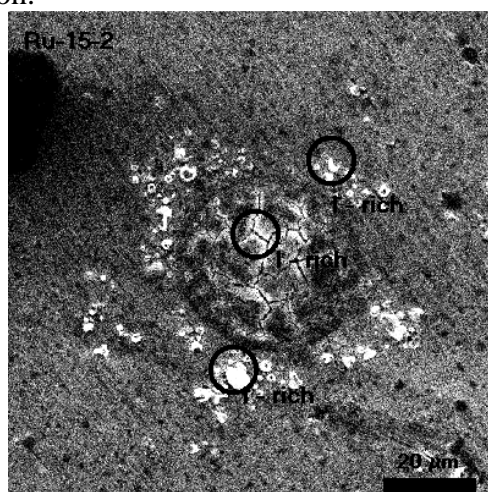

Figure 27: Surface of the nickel holder of sample No. Ru-15-2. at a digital BE image with 900-times of magnification

The small sized globular and slightly elongated grains shown in the above figure contained I and Ru (probably together with O).

On the *Si sample holder* of this sample more grains could be found than on the Si holder of the preceding sample. Some examples of these grains are illustrated in two BEI of Figure 28. The left hand side image has shown grains with various compositions, from them two were magnified on the right hand side image taken at 4000-times of magnification. In the upper part of the latter image a small grain can be seen with Nd, low amounts of Zr, Se and Te content, while the one present in the lower part, contained Zr, Se, Ru and probably small amounts of Te. This grain is shown in the middle of the left hand side image, too.
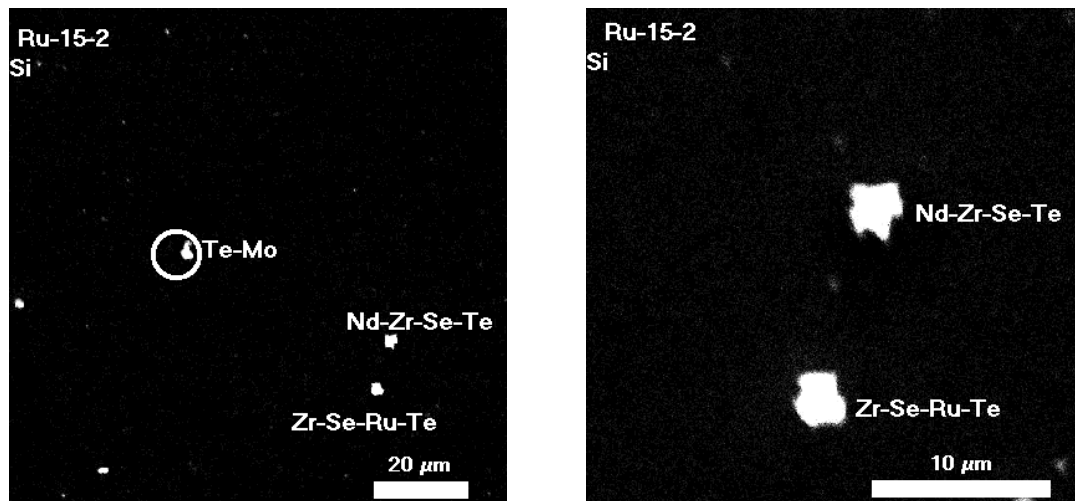
Figure 28: Two digital BE images showing grains with various elemental composition for Si holder of sample No. Ru-15-2

Sample collected on quartz filter contained a lot of grains with various compositions. Most of the grains were Zr (oxide), their shape was globular, and some of them rectangular (see the image on the left hand side of Figure 29). We found Zr-rich aggregate; from which small amounts of Ru, Fe and Cr could be detected (the latter two elements were probably impurities), too. Beside Zr Ru and Se, or Nd, Ru and Se, or Ru, Te and Se could be found in some other grains. We found an aggregate with Zr, Nd, Te and small amounts of Ba content.
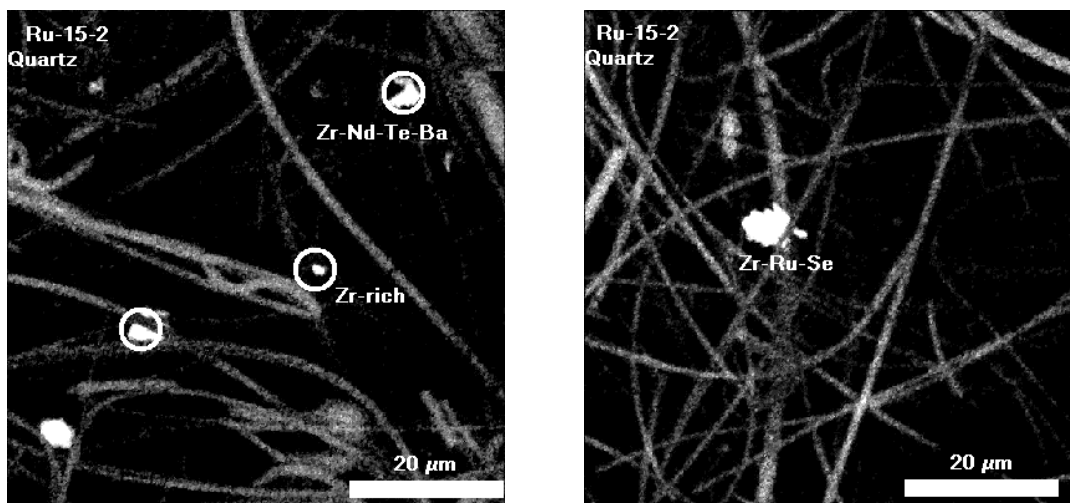

Figure 29: Two typical BE images showing grains with various elemental compositions

Typical BE images can be seen in Figure 30, where grains with various compositions – e.g. Zr, Nd, Ru and Se content – are presented. However most of the grains were Zr-rich.
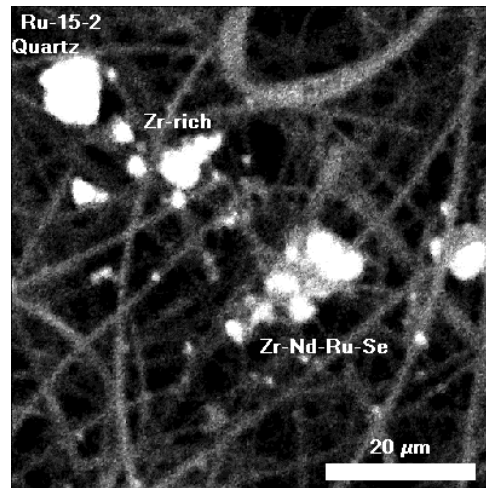
Figure 30: BEI showing grains with various elemental compositions for quartz filter of sample
No. Ru15-2

Sample Ru15-3: *On the Ni and Si sample holders* we did not find grains and deposited particles. *On the quartz filter* there were a few grains, which contained some impurities (Fe, Cr, Ni, Ti), too. We found 2 or 3 grains which contained I, Ni and small amounts of Ru and probably Mo. Figure 31 taken at 800-times of magnification shows such grains.
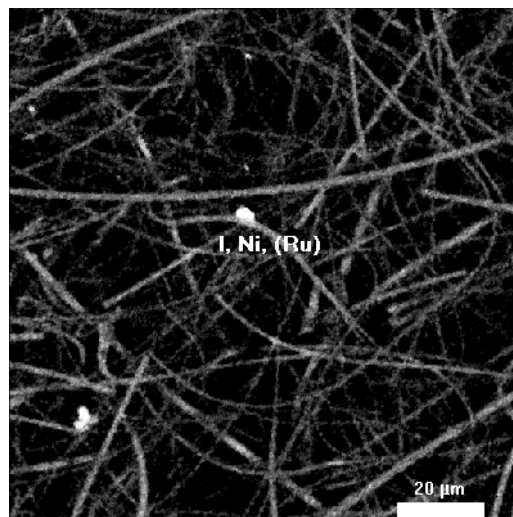

Figure 31: BEI showing the surface of quartz filter of sample No. Ru15-3

By summarizing the above findings, we could state, that iodine deposited mostly on the Ni sample holder. On the Si holder only less amounts of iodine could be found, while on the quartz filter iodine deposited rarely. On the Ni holder corrosion spots were formed for the effect of iodine. Iodine could be detected on the corrosion spots. Ru was present together with some oxygen. In the neighbourhood of the corrosion spots iodine was enriched in form of globular or irregular grains. From the other elements of the fission products only those could be detected which had lower melting points, such as Se and Te. Other elements like Cd and Ag could not be found probably due to their small quantities. It could be stated, that by progressing of the experiment duration mostly the amount of iodine decreased, other elements (e.g. Se, Te, Cs) were present in samples 2.

4.4 Ru powder in ZrO$_2$ with other FP products and UO$_2$ (Ru18, Ru19)

At these two tests 100 mg UO$_2$ were given to the charge of ZrO$_2$ and FP elements. (This amount was a so called free treatment quantity, allowed to work with in a laboratory not qualified for work with radioactive materials.) The high chemical stability of ZrO$_2$ results, that it has no influence on the oxygen potential, it is determined by the other compounds.

At Ru18 experiment wet air with ca 5% steam was applied, at Ru19 dry air was used. Similar to experiments, where not only Ru but other fission products were in the charge, the escape of ruthenium were taken place with some delays. The delay was larger at using wet air. If UO$_2$ were in the charge the partial pressure of Ru oxides were higher as in the case of Ru powder or Ru powder + fission products.

In the quartz filter in the inlet tube of first sampler at Ru18 (wet air) appeared a black precipitation. The XRF investigation proved it to be Se with a small amount of Mo and Ru. On the further filters it did not formed. Using dry air appeared on the first filter (19-1) a similar, but brown precipitation. It had also Se content with some other FP elements.

At the end of Ru18 and Ru19 experiments the ZrO$_2$ matrix was not so white, as before, but had a slight brown color. It was certainly from BaUO$_4$, which is forming from BaCO$_3$ and UO$_2$ at temperatures higher than 1000°C.

After a longer time both with dry and wet air the average partial pressure of RuO$_4$ has been about 2.10^{-6} bar.

4.5 Control test for the role of oxygen (Ru11)

Even if it is quite obvious, that the Ru evaporate at high temperatures as oxides formed at the presence of oxygen gas a control test has to be made to exclude any artificial effect. The test was made by usual method applied for the experiments, 5 mg Ru powder in ZrO$_2$ matrix. At this test high purity argon was used instead of air. At first for a longer time argon was flowing through the reaction chamber, when it was not yet in the hot area. After thorough flushing the reaction chamber was sank into the hot area of furnace. At first dry air was used for 2 hours, after that it was changed to wet air. No Ru appeared in the sampler or on the outlet inlet tube.

4.6 Deposits on the inlet tubes

As it was mentioned earlier at the decreasing temperature section of outlet tubes ruthenium dioxide deposits were formed. About 70-90 % of ruthenium oxides were transformed to RuO$_2$. The segregation is going from the temperature of formation (1100°C) down to about 600-700 °C. With decreasing temperature the rate of

$$RuO_4 \rightarrow RuO_2 + O_2$$
$$RuO_3 \rightarrow RuO_2 + 1/2\ O_2$$

processes are slowing down and at the lower temperature mentioned entirely stops. In Figure 32 the picture of deposits of Ru16-1 and Ru16-2 inlet tubes and quartz rods can be seen. (At this experiment the inlet tubes together with the rods can be seen. The temperatures at the end of deposition determined from the position and thermocouple calibration (Figure 5) compared to those calculated from partial pressure of ruthenium oxides (Table I/2) agree reasonable well.
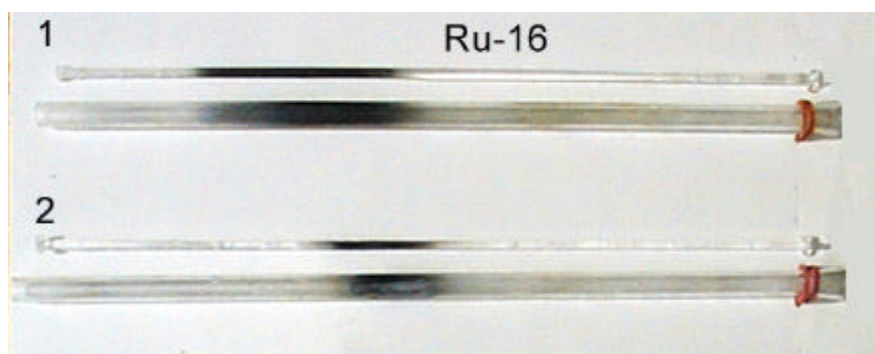

Figure 32. Deposits on inlet quartz tubes and rods from Ru16-1 and Ru16-2
(Times of sampling: (1) 0-30 min., (2) 30-60 min.)

In Figure 33 the morphology of crystallic deposit of an inlet tube is shown. The left side was the high temperature, the right the low temperature part. At the high temperature part crystals with near spherical shape have been found, further to the lower temperature part needle shaped crystals growing from a center on the tube wall. At the lower temperature end again sphere shaped larger species, further microcrystallic deposits can be seen.

Figure 33. RuO_2 crystals inside an inlet quartz tube.

4.7 Summary on partial pressure results of RuO₄ in outlet air

The summary of results regarding the partial pressure of RuO_4 in the outlet air are summarized on the next two plots.

In Figure 34 the test results with Ru powder in ZrO_2 are shown. The temperature of reaction chamber (air - Ru reaction) was 1100 °C at all experiments except the two tests signed on the plot (1000 and 1200 °C). The more effective evaporation at start of experiments results a higher RuO_4 partial pressure in the escaping air. At larger concentration in high temperature air remains a higher concentration after the cooling down, because the rate of RuO_4 - RuO_2 process is not fast enough to follow perfectly the equilibrium with the temperature. The rate of equilibrium process is slowing down with the temperature and stops at about 600 - 700 °C. That means that the ca 10^{-6} bar escaping partial pressure is not an equilibrium value at ambient temperature (it would be about 10^{-10} bar). Some other phenomena at the experiment, precipitations on surfaces along the outlet way of gas because of some catalytic effect support this assumption.
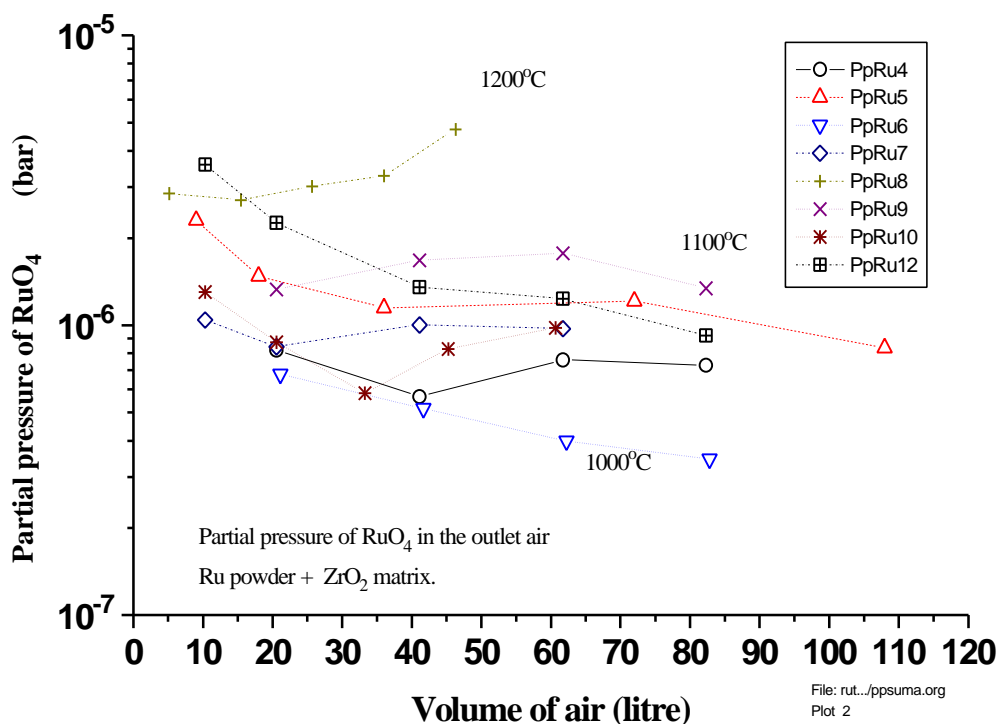

Figure 34. Partial pressure of RuO_4 in outflow air at $Ru + ZrO_2$ experiments

At experiments with other fission products in the charge the escape of ruthenium tetroxid showed some delay (Figure 35). The XRF investigation of precipitates on the quartz rods proved the reason of the effect (Figure 11).
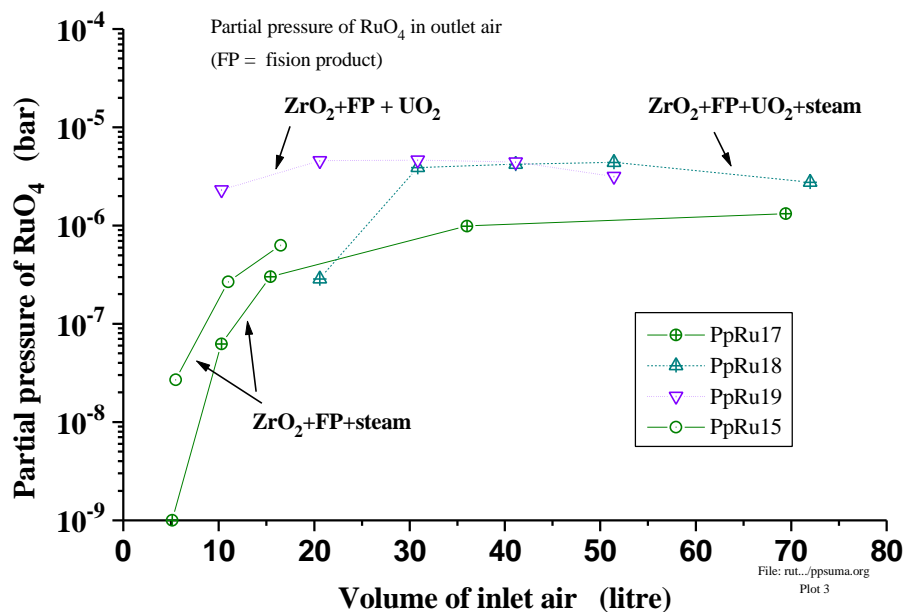
Figure 35. Partial pressure of RuO$_4$ in outflow air at experiments with charge
Ru + ZrO$_2$ + fission products and also with UO$_2$.

The CsI evaporate faster than the Ru oxides and form a layer at a level above the ruthenium dioxide, presumable as CsOH or Cs$_2$O. The Cs compounds are absorbing the Ru-oxides as ruthenates at the beginning of experiment. The ruthenium oxides can flow out with the air only if the Cs compounds are converted to ruthenates. (At these experiments I$_2$ appeared in the absorber solution at the beginning, after that it was flushed away by the streaming air.) After longer time the partial pressure of RuO$_4$ is going to about 1.10^{-6} bar.

If the charge in the reaction chamber contained UO$_2$ as well beside the fission products the delay effect appeared again but just after it the Ru escape was faster, the partial pressure of oxides raised to 4.10^{-6} bar. After longer time it was going back to the usual 1.10^{-6} bar. It seems so, that the steam content in air has some influence for the delay, maybe by enhancing the evaporation of molybdenum. After a longer time there is no difference in the escape rate of ruthenium in wet or dry air.

4.8 Results compared with data from hot particles collected after Chernobyl accident

During the Chernobyl accident a large part of burned out fuel was in contact with hot air. The escape of volatile fission product elements was increased by the strong high temperature oxidation, a similar effect we were dealing with in the frame of the present project.

After the accident aerosol samples were investigated in our Institute (at that time KFKI) collected in the filter system a large facility [23]. Detailed data were published about 15 hot particles with radioactivity larger than 10 Bq. They found 3 particles containing only Ru as active element, but the other 12 had also Ru as component.

The 3 particle containing only Ru as radioactive element had activities as 29, 570 and 133 Bq. If they would not contain other elements as Ru their size would be 0.61, 1.6 and 1.0 μm, presumed spherical shape with density of 7.0 g/cm^3, and taking into account the non active Ru isotopes as well [24]. On the basis of experiences we got during the present work we think as so, that the partial pressures of Ru-oxides in the rising up and at the same time cooling down gas were oversaturated and changed toward the chemical equilibrium by the catalytic effect of small RuO_2 particles. The catalytic effect specific and the growing of RuO_2 particles by using RuO_4 gas has been preferred.

At the further 12 particles Cs, Ba, La and Ce has been found. According to the calculations using their activity the joint number of the atoms mentioned was usually 1-2, at the highest 4.4 related to the number of Ru atoms. We can assume, that the evaporation of these particles was in the form of ruthenates as was supposed by Cordfunke et al. [25].

5. SUMMARY AND CONCLUSIONS

In the late phase of a reactor accident or during refuelling incidents the degraded high temperature core can get into contact with air. Following the oxidation and failure of zirconium cladding the interactions of fuel pellets with air lead to the formation of some volatile fission product compounds. Ruthenium exists in the irradiated fuel in form of metallic – non-volatile – inclusions, which can be oxidized by air into volatile ruthenium-trioxide and ruthenium-tetroxide. The release of radioactive [103]Ru and [106]Ru significantly increases the source term, for ruthenium is one of the most frequent fission products and large amount of this element is present in the reactor core.

The oxidiation and release of ruthenium was investigated in very few experiments. Integral air ingress tests were carried out in the AEKI, but the fuel rods contained no fission product elements [26,27,28]. In the present work the oxidation and release of ruthenium was investigated in small scale experiments. The main obrsevations and results of the tests are the followings:

- under high temperature conditions in air atmosphere the total amount of ruthenium was released from the furnace,
- max. 10% of ruthenium reached the room temperature samplers during the total experimental time (several hours)
- most of the formed ruthenium-oxides deposited on the surface of outlet tube from the furnace at 600-700 ^{o}C,
- in the later phase of the tests the ruthenium-tetroxide was formed and released from the deposited ruthenium-dioxide
- the presence of other fission products delayed the release of ruthenium, but did not decrease the released mass.

On the basis of the described experiments conservative estimation can be given on the release of ruthenium in high temperature air ingress conditions. In the case of a reactor accident the contact between the air atmosphere and the fission products is limited and so the release may take longer time. For this reason additional experiments will be carried out to investigate the retention mechanism of fuel pellets and support the integral bundle tests.

The experiments carried out till now indicates that in the air ingress phase of a severe accident most of the ruthenium will be oxidised and released in form of volatile oxides from the reactor core. Most of the released ruthenium will deposite on the cold temperature surfaces of the primary circuit and containment. The ruthenium release will be continued if high temperature air flow through these surfaces, the release rate can be estimated as 10^{-6} bar partial ruthenium-oxide pressure. The injection of KOH or NaOH solution could be suggested as accident management measure in order to decrease the release rate.

ACKNOWLEDGMENTS

REFERENCES

[1]   G. W. Parker, C.J. Barton, G. E. Creek, W. J. Martin and R. A. Lorenz, *Out-of-Pile Studies of Fission-Product Release from Overheated Reactor Fuels at ORNL*, 1955-1965, ORNL-3981, Oak Ridge National Laboratory, Oak Ridge, TN, July (1967).

[2]   F. C. Iglesias, C. E. L. Hunt, F. Garisto and D. S. Cox, *Measured Release Kinetics of Ruthenium from Uranium Oxides in Air*, Proc. Int'l. Seminar on Fission Product Transport Processes During Reactor Accidents, J. T. Rogers, editor, Hemisphere Publishing Corp., Washington, D. C., (1990).

[3]   F Garisto, F. C. Iglesias and C. E. L. Hunt, *A Thermodynamic/Mass Transport Model for the Release of Ruthenium from Irradiated Fuel*, Proc. Int'l. Seminar on Fission Product Transport Processes During Reactor Accidents, J. T. Rogers, editor, Hemisphere Publishing Corp., Washington, D. C., (1990).

[4]   C. E. L. Hunt, F. C. Iglesias and D. S. Cox, *Measured Release Kinetics of Iodine and Cesium from UO_2 at High Temperatures Under Reactor Accident Conditions,* Proc. Int'l. Seminar on Fission Product Transport Processes During Reactor Accidents, J. T. Rogers, editor, Hemisphere Publishing Corp., Washington, D. C., (1990).

[5]   R. Williamson and S. A. Beetham, *Fission Product Release During the Air Oxidation of Irradiated Uranium Dioxide*, Proc. Int'l. Seminar on Fission Product Transport Processes During Reactor Accidents, J. T. Rogers, editor, Hemisphere Publishing Corp., Washington, D. C., (1990).

[6]   H. Albrecht, *Freisetzung von Spalt- und Aktivierungsprodukten beim LWR-Kernschmelzen,* KfK 4264 Report, Karlsruhe, (1987).

[7]   R. Gandon, D. Boust and O. Bedue, *Ruthenium Complexes Originating from the Purex Process: Coprecipitation with Copper Ferrocyanides via Ruthenocyanide Formation*, Radiochimica Acta 61, 41-45. (1993).

[8]   H. Longley and W. L. Templeton, *Marine Environmental Monitoring in the Vicinity of Windscale*, Radiologycal Monitoring of the Environment (ed. J. K. Jones), Pergamon Press, Oxford (1965).

[9]   F. A. Fry, R. H. Clarke and M. C. O'Riordan, *Early Estimates of UK Radiation Doses from the Chernobyl Reactor*, Nature 321, 193-165. (1986).

[10]   H. O. Denschlag, A. Diel, K. H. Glasel, R. Heimann N. Kaffrel, U. Knitz, H. Menke, N. Trautmann, M. Weber and G. Herrmann, *Fallout in the Mainz Area from the Chernobyl Reactor Accident*, Radiochimica Acta 41, 163-172. (1987).

[11]   P. Hoffmann, N. Pliz, K. H. Leiser V. Ilmstader and M. Griesbach, *Radionuclids from the Chernobyl Accident in the Environment of Chattia, a Region of the FRG*, Radiochimica Acta 41, 173-179. (1987).

[12] H. Toivonen, R. Pöllanen, A Leppanen, S. Klemola, J. Lahtinen, K. Servomaa, A. L. Savolainen and I. Valkama, *A Nuclear Incident at a Power Plant in Sosnovyy Bor, Russia*, Health Phys. <u>63</u>, 571-573. (1992).

[13] J. S. Punni, P. K. Mason. *UO$_2$ oxidation and volatilization,* AEAT-1277 Report, Harwell, (1998).

[14] H. Albrecht. *Radioactivity emission from the Chernobyl accident,* Radiochimica Acta <u>41</u>. (1987).

[15] R. Pöllanen, *Highly Radioactive Ruthenium Particles Released from the Chernobyl Accident: Particle Characterisation and Radiological Hazard*, Radiat. Prot. Dosim. <u>71</u>, 23-32. (1997).

[16] W. Hofmann, D. J. Crawford-Brown and T. B. Martonen, *The Radiological Significance of Beta Emitting Hot Particles Released from the Chernobyl Nuclear Power Plant*, Radiat. Prot. Dosim. <u>22</u>, 149-157. (1988).

[17] Gmelins Handbuch der Anorganischen Chemie, *Ruthenium*, <u>63</u>. Erg-band, Verlag Chemie GMBH, Weinheim/Bergstr., (1970).

[18] C. B. Alcock, G. W. Hooper, Proc. Royal Soc. (London), <u>A-254</u>. 551. (1960).

[19] W. L. Phillips, Am. Soc. Metals Trans. Quart. <u>57</u>. 33-37. (1964).

[20] E. D. Marshall, R. R. Rickard, Anal. Chem. <u>22</u>. 795-797. (1952).

[21] W. L. Belew, G. R. Wilson, L. T. Corbin, Anal. Chem. <u>33</u>. 886-888. (1961).

[22] C. V. Banks, J. W. Ö' Laughlin, Anal. Chem. <u>29</u>. 1412-1417. (1957).

[23] I. Balásházy, I.Fehér, G.Szabadyné-Szende, M. Lorinc, P. Zombori, L. Pogány, Radiation Protection Dosimetry, <u>22</u>, No.4. 263-267 (1988)

[24] Vértes Péter (AEKI) private communication.

[25] E.H.P. Cordfunke, R.J.M. Konings, S.R.M. Meyssen: Vapor pressure of some cesium compounds II. Cs$_2$MoO$_4$ and Cs$_2$RuO$_4$, ECN-RX-91-011, Netherlands Energy Research Foundation, Petten, The Netherlands, February 1991.

[26] Z. Hózer, P. Windberg, I. Nagy, L. Maróti, L. Matus, M. Horváth, A. Pintér, A. Czitrovszky, P. Jani: CODEX-AIT-1 Experiment: Core Degradation Test Under Air Ingress, KFKI-2002-02/G, Budapest, 2002

[27] Z. Hózer, P. Windberg, I. Nagy, L. Maróti, L. Matus, M. Horváth, A. Pintér, Á. Griger, M. Balaskó, B. Alföldy, A. Czitrovszky, P. Jani: CODEX-AIT-2 Experiment: Core Degradation Test With Steam Oxidation And Air Ingress, KFKI-2002-03/G, Budapest, 2002

[28] Z. Hózer, P. Windberg, I. Nagy, L. Maróti, L. Matus, M. Horváth, A. Pintér, M. Balaskó, A. Czitrovszky, P. Jani: Interaction of Failed Fuel Rods Under Air Ingress Conditions, Nuclear Technology, vol. 141, March 2003